Running Head: PRX01, PRX44 and PRX73 are extensin-related peroxidases active in root hair growth

Authors for Correspondence:
José M. Estevez
Fundación Instituto Leloir, Av. Patricias Argentinas 435, Buenos Aires C1405BWE, Argentina. TE: 54-115238-7500 EXT. 3206
Centro de Biotecnología Vegetal, Facultad de Ciencias de la Vida, Universidad Andrés Bello and Millennium Institute for Integrative Biology (iBio), Santiago CP 8370146, Chile.
Email: jestevez@leloir.org.ar / jose.estevez@unab.cl

Research area most appropriate for paper: Plant Biology

Text Word count: 3,565
Figures 1-5
Experimental procedures
References: 68

19 **RESEARCH REPORT**

20 **PRX01, PRX44, and PRX73 are Class-III extensin-related peroxidases that modulates root hair**
21 **growth in *Arabidopsis thaliana***

22

23 Eliana Marzol[1,#], Cecilia Borassi[1,#], Philippe Ranocha[2], Alejandro Aptekman[3,4], Mauro Brindas[5],
24 Janice Pennington[6], Julio Paez-Valencia[6], Javier Martínez Pacheco[1], Diana Rosa Rodríguez Garcia[1],
25 Yossmayer Rondon[1], Mariana Carignani[1], Silvina Mangano[1], Margaret Fleming[7], Francisca Blanco-
26 Herrera[8,9], Patricia Bedinger[7], Christophe Dunand[2], Luciana Capece[5], Alejandro Nadra[3,4], Michael
27 Held[10], Marisa Otegui[6,11] & José M. Estevez[1,8,†]

28

29

30 [1]Fundación Instituto Leloir and IIBBA-CONICET. Av. Patricias Argentinas 435, Buenos Aires
31 C1405BWE, Argentina.
32 [2]Université de Toulouse, UPS, UMR 5546, Laboratoire de Recherche en Sciences Végétales, F-31326
33 CNRS, UMR 5546 Castanet-Tolosan, France.
34 [3]Departamento de Fisiología, Biología Molecular y Celular, Facultad de Ciencias Exactas y Naturales,
35 Universidad de Buenos Aires, Ciudad Universitaria, Buenos Aires C1428EGA, Argentina.
36 [4]Departamento de Química Biológica, Facultad de Ciencias Exactas y Naturales, Universidad de
37 Buenos Aires (IQUIBICEN-CONICET), Ciudad Universitaria, Buenos Aires C1428EGA, Argentina.
38 [5]Departamento de Química Inorgánica, Analítica y Química Física, Facultad de Ciencias Exactas y
39 Naturales, Universidad de Buenos Aires (INQUIMAE-CONICET), Buenos Aires, CP. C1428EGA,
40 Argentina.
41 [6]Laboratory of Cell and Molecular Biology, University of Wisconsin, Madison, WI, USA.
42 [7]Department of Biology, Colorado State University, Fort Collins, Colorado 80523-1878, USA.
43 [8]Centro de Biotecnología Vegetal, Facultad de Ciencias de la Vida, Universidad Andrés Bello and
44 Millennium Institute for Integrative Biology (iBio), Santiago, Chile.
45 [9]Center of Applied Ecology and Sustainability (CAPES), Chile.
46 [10]Department of Chemistry and Biochemistry, Ohio University, Athens, OH 45701, USA.
47 [11]Departments of Botany and Genetics, University of Wisconsin, Madison, WI, USA.

48

49 [#]co-first authors
50 [†] Correspondence should be addressed. Email: jestevez@leloir.org.ar / jose.estevez@unab.cl (J.M.E).

51

52 Key words: Arabidopsis, cell walls, extensins, root hairs, ROS, class-III peroxidases.

Abstract

Root hair cells acts at the root surface as important sensors of soil conditions. Root hairs are able to expand several hundred times their original size in a couple of hours to reach and uptake water-soluble nutrients. This fast and oscillating growth requires a continuous remodelling of the cell wall to allow for the root hair to expand in a tightly controlled manner. Root hair cell walls contain polysaccharides and hydroxyproline-rich glycoproteins (HRGPs) including extensins (EXTs). Class-III peroxidases (PRXs) are secreted into the apoplastic space and are thought to trigger either cell wall loosening mediated by oxygen radical species, or polymerization of cell wall components including the Tyr-mediated assembly of an EXT network (EXT-PRXs). The precise role of each of these EXT-PRXs remains to be discovered. By using genetic, biochemical and modeling approaches we have identified and characterized three root hair specific EXT-PRXs, PRX01, PRX44, and PRX73. The triple mutant *prx01,44,73* as well as the overexpressors for PRX44 and PRX73 showed opposite effect on root hair growth, peroxidase activity, ROS-production, cell wall thickness, and Tyr-crosslinks in EXTs. These results suggest a key role of these three EXT-PRXs in the control of root hair growth linked to cell wall properties during polar cell expansion. Finally, modeling and docking calculations have suggested these three EXT-PRXs might be able to interact with non-*O*-glycosylated sections of EXT peptides that reduced Tyr-to-Tyr intra-chain distances in EXT aggregates and might enhance Tyr-crosslinks.

Word count: 236

Introduction

Primary cell walls composed by a diverse network of polysaccharides and structural glycoproteins, regulate cell elongation, which is crucial for several plant growth and developmental processes. Extensins (EXTs) belong to hydroxyproline (Hyp)-rich glycoprotein (HRGP) superfamily and broadly include related glycoproteins such as proline-rich proteins (PRPs) and leucine-rich repeat extensins (LRXs) with multiple Ser-$(Pro)_{3–5}$ repeats that may be *O*-glycosylated and contain Tyr (Y)-based motifs (Marzol et al. 2018). EXTs require several modifications before they become functional (Marzol et al. 2018). First, they are hydroxylated and *O*-glycosylated in the secretory pathway and then, secreted *O*-glycosylated EXTs are crosslinked and insolubilized in the plant cell wall by the activity of secreted class-III peroxidases (PRXs) on the Tyr-based motifs (Lamport et al., 2011; Marzol et al. 2018). PRXs are thought to facilitate both intra and inter-molecular covalent Tyr–Tyr crosslinks in EXT networks possibly thought the assembly of triple helices (Velasquez et al. 2015) by generating *iso*dityrosine units (IDT) and pulcherosine, or di-*iso*dityrosine (Di-IDT), respectively (Brady et al., 1996; 1998). However, the underlying molecular mechanisms of EXT cross-linking and assembly have not yet been determined. The presence of Tyr-mediated crosslinking in EXT and related glycoproteins allow them to form a dendritic glycoprotein network in the cell wall. This network affects *de novo* cell wall formation during embryo development (Cannon *et al.*, 2008), in polar cell expansion processes in root hairs (Baumberger 2001, 2003; Ringli 2010; Velasquez et al. 2011, 2015a,b) and pollen tubes (Sede et al. 2017; Ringli et al. 2017; Wang et al. 2017).

Apoplastic class-III PRXs are heme-iron-dependent proteins, member of a large multigenic family in land plants, with 73 members in *Arabidopsis thaliana* (Passardi et al. 2004; Weng and Chapple, 2010). These PRXs catalyzed several different Classs of reactions. PRXs activities coupled to $_{apo}$ROS molecules ($_{apo}H_2O_2$) directly affect the degree of cell wall crosslinking (Dunand et al. 2007) by oxidizing cell wall compounds and leading to stiffening of the cell wall through a peroxidative cycle (PC) (Lamport et al. 2011). On the other hand, $_{apo}$ROS coupled to PRX activity enhances non-enzymatic cell wall-loosening by producing oxygen radical species (e.g., $^{\bullet}OH$) and promoting growth in the hydroxylic cycle (HC). It is unclear how opposite effects on cell wall polymers are coordinated during plant growth (Passardi et al. 2004, Cosio & Dunand 2009). Finally, PRXs also contribute to the superoxide radical ($O_2^{\bullet-}$) pool by oxidizing singlet oxygen in the oxidative cycle (OC), thereby affecting $_{apo}H_2O_2$ levels. Thus, several PRXs are involved in the oxidative polymerization of monolignols in the apoplast of the lignifying cells in xylem (e.g. PRX017; Cosio et al 2017), in the root endodermis (e.g. PRX64; Lee et al. 2013; Ropollo et al. 2011), and in petal detachment (Lee et al 2018). In addition, PRXs are also able to polymerize other components of the plant cell wall such as suberin, pectins, and EXTs (Schnabelrauch *et al.*, 1996; Bernards et al., 1999; Jackson et al., 2001; Francoz et al. 2019). Although several candidates of PRXs have been associated specifically to EXT-crosslinking (EXT-PRXs) by *in vitro* studies (Schnabelrauch et al., 1996; Wojtaszek et al., 1997; Jackson et al., 2001; Price et al., 2003; Pereira et al. 2011; Dong et al., 2015; Jacobowitz et al. 2019),

111 the *in vivo* characterization and mode of action of these EXT-PRXs remain largely unknown. In this
112 work, using a combination of reverse genetics, molecular and cell biology, computational molecular
113 modeling, and biochemistry, to identify three apoplastic PRXs, PRX01, PRX44 and PRX73, as key
114 enzymes for Tyr-crosslinking of cell wall EXTs in growing root hair cells. In addition, we propose a
115 model where *O*-glycosylation levels on the triple helixes of EXTs may regulate the degree of Tyr-
116 crosslinking affecting the expansion properties of cell walls as suggested before (Velasquez et al.
117 2015a). Our results open the way for the discovery of future similar interactions during root hair
118 development and in response to the environment changes such oscillating nutrients availability in
119 the soil.
120
121 **Results and Discussion**
122 In this work, we have chosen to analyze root hair cells because they are an excellent model to track
123 cell elongation and to identify PRXs involved in the EXT assembly. Previously, it was suggested that
124 single mutants for *pxr1*, *prx44* and *prx73* were involved in root hair growth and ROS homeostasis
125 (Mangano et al. 2017). All three PRXs are under the transcriptional regulation of the root hair
126 specific transcription factor RSL4 (Menand et al. 2007) although their mechanisms of action
127 remained to be characterized (Mangano et al. 2017). As expected, these three PRXs are also highly
128 co-expressed with other root hair specific genes enconding cell wall EXTs (e.g. EXT6-7, EXT12-14 and
129 EXT18) and EXT-related glycoproteins (e.g. LRX1 and LRX2), which are important for cell expansion
130 (Ringli 2010; Velasquez et al. 2011; Velasquez et al. 2015b) (**Figure S1**). Based on this evidences, we
131 hypothesized that these three PRXs might be EXT-PRXs and perform the Tyr-crosslinks to catalyze
132 the EXT assembly in root hair cell walls.
133
134 We first made transcriptional GFP-tagged reporters of PRX01, PRX44 and PRX73 promoter regions to
135 confirm their specific expression in root hairs. In agreement with the *in silico* database (Mangano et
136 al. 2017 and **Figure S1**), all of them were strongly expressed in root hair cells during cell elongation
137 (**Figure 1A**). Single and double combinations of mutants for these three PRXs did not show
138 abnormal root hair growth (Mangano et al. 2017) suggesting a high degree of functional
139 redundancy. Then, we obtained the triple null mutant *PRX01,44,73* (**Figure 1B**) as well as two
140 independent lines overexpressing each of the PRXs fused to GFP and under the strong *35SCaMV*
141 promoter (PRX^{OE}) to test whether the expression levels of PRXs affect the normal root hair growth.
142 Whereas the *prx01,44,73* mutant showed much shorter root hair cells (**Figure 1B**) than the
143 previously reported for each of the individual *prx* mutants (Mangano et al. 2017), both independent
144 lines of $PRX44^{OE}$ and $PRX73^{OE}$ showed significant longer root hairs than the Wt Col-0 control (**Figure**
145 **2A-B**). $PRX01^{OE}$ lines, however, failed to enhance root hair growth when compared to Wt Col-0
146 (**Figure 2A-B**). We reasoned that the lack of enhanced root hair expansion in $PRX1^{OE}$ could be due to
147 reduced expression compared to the PRX44 ^{OE} and PRX73 ^{OE} lines. However, both by detection of
148 GFP signal in intact roots (**Figure 2C**) and immunoblot analysis of protein extracts with anti-GFP

149 antibodies (**Figure 2D**), we found that PRX1-GFP and PRX44-GFP are strongly expressed whereas
150 PRX73-GFP showed a more moderate expression; the three PRX GFP-fusion proteins were detected
151 the expected molecular weight (**Figure 2D**), indicating that the tagged proteins are stable. These
152 results together highlight partially redundant but not identical roles of PRX1, PRX44 and PRX73 as
153 positive regulators of polar growth. This is in agreement with the negative effect of SHAM, which
154 blocks the peroxidase activities of most peroxidases, on root hair growth (Mangano et al. 2017).
155 Therefore, we measured *in vitro* total peroxidase activity using a guaiacol oxidation-based assay and
156 found that *prx01,44,73* roots showed reduced peroxidase activity (close to 50% reduction) (**Figure**
157 **1C**) while PRXs^{OE} lines showed enhanced activity, with a 40-50% increase in PRX73^{OE} and
158 approximately 20% increase in PRX44^{OE} (**Figure 2E**). Consistent with our root hair growth analysis
159 (**Figure 2A**), the PRX01^{OE} lines showed no or moderate increased peroxidase activity (**Figure 2E**). We
160 then measured cytoplasmic ROS ($_{cyt}$ROS) levels by oxidation of H_2DCF-DA and apoplastic ROS
161 ($_{apo}$ROS) levels with the Amplex Ultra Red (AUR) probe in root hair tips. The *prx01,44,73* root hair
162 tips showed lower levels of $_{cyt}$ROS (**Figure 1D**) but increased $_{apo}$ROS accumulation (**Figure 1E**)
163 compared to Wt Col-0. The $_{apo}$ROS levels were similar in PRX01,44,73^{OE} lines when compared to Wt
164 Col-0 (**Figure 2F**). These results suggest a possible role of PRX01, PRX44 and PRX73, as apoplastic
165 regulators of ROS-linked root hair cell elongation, possibly related to EXT assembly in the cell walls.
166 These three PRXs consume ROS, most probably H_2O_2, for its catalytic functions in the cell wall-
167 apoplast.
168
169 Next, we designed an EXT reporter to track changes between EXT secretion and insolubilization in
170 the cell walls mediated by PRXs during root hair cell elongation. The secreted EXT-reporter carries a
171 Tomato tag (SS-TOM-Long-EXT) that is resistant to acidic pH (Shen et al. 2014) typical of plant cell
172 walls and apoplastic spaces (Stoddard & Rolland 2018). A secreted Tomato tag (ss-TOM) was used as
173 a control (**Figure S3A**). EXT expression was first monitored in onion cells (**Figure S3**), and then was
174 stably expressed in *Arabidopsis* root hairs (**Figure S2C**). In both cases, plasmolysis was used to
175 retract the plasma membrane from the cell surface showing that the EXT-reporter was localized in
176 the cell walls. By performing western blot analysis, we detected the full length EXT-Tomato fusion
177 protein with possible *O*-glycans modifications running as higher molecular weight bands; the control
178 SS-TOM was detected at the expected size (**Figure S2B**). More importantly, the EXT-reporter did not
179 interfere with the polar growth of root hairs (**Figure S2D**), and therefore, was used it to track
180 changes in the *in situ* arrangement of cell wall EXTs. Then, we tested if SHAM, a peroxidase inhibitor
181 known to impair root hair growth (Mangano et al. 2017), might affect the secretion and assembly of
182 SS-TOM-Long-EXT into the new formed apical root hair cell wall (**Figure 3A-B**). SHAM treatment not
183 only disrupted polar cell expansion in root hairs as previously shown (Mangano et al. 2017) but
184 more importantly, triggered an abnormal EXT deposition in the apical cell walls suggesting that Tyr-
185 crosslinks might be affected (**Figure ?**). To further analyze the ultrastructure of the cell wall in
186 growing root hairs, we analyzed Wt Col, PRX44^{OE}, and *prx01,44,73* triple mutant roots treated with

187 or without SHAM by transmission electron microscopy (**Figure 3A**). Whereas there was no
188 statistically significant difference between cell wall thickness at the root hair tips of PRX44^{OE} and Wt
189 Col-0 plants (1.2 ±0.3 µm s for Wt and 1.05 ±0.11 µm for PRX44^{OE}), the *prx01,44,73* root hairs had
190 much thinner cell walls (0.4 ±0.4 µm) (**Figure 3B**). In the three genotypes, SHAM treatment caused a
191 slight increase in cell wall thickness that was only statistically significant in the PRX44^{OE} root hairs
192 (**Figure 3B**).
193
194 We then measured the levels of EXT cross-links at Tyr units in isolated whole roots by measuring
195 peptidyl-tyrosine (Tyr) and iso-dityrosine (IDT) (dimer of Tyr). We did detect significant differences
196 in the peptidyl-Tyr between Wt Col-0 and *prx01,44,73* triple mutant while slightly higher levels on
197 IDT in extracted EXTs from PRX73^{OE} line (**Table S1**). On the other hand, strong down-regulation of
198 Tyr- and IDT-levels were found in miss-glycosylated EXTs mutants like *p4h5 sergt1-1* and *sergt1-1*
199 *rra3* (**Table S1**) suggesting a strong impact of *O*-glycans on EXT Tyr crosslinking as previously
200 suggested based on their drastic reduced root hair growth (Velasquez et al 2015a). We hypothesize
201 that absent or low *O*-glycosylation levels on EXTs or a change in PRX levels may trigger a reduction in
202 the amount of peptidyl-Tyr and IDT on EXTs with a putative concomitant increase in the amounts of
203 higher Tyr-crosslink units (trimers and tetramers) thus impacting on root hair growth. Further
204 research is needed to understand the *in vivo* regulation of Tyr-crosslinking of EXTs by PRXs in plant
205 cells.
206
207 One of the major limitations in our understanding of how EXT function in the plant cell walls is the
208 lack of a realistic full-length EXT protein model. Previously, we have generated preliminary versions
209 of a short EXT triple helix model (Velasquez et al. 2015a). To have a more detailed understanding of
210 how EXT molecules might behave in the plant cell wall, we have built a larger model of a triple helix
211 EXT sequence that includes 10 conserved repeats (SPPPPYVYSSPPPPYYSPSPKVYYK) with a total
212 length of 750 amino acids (250 in each polypeptide chain) by using a coarse grained molecular
213 dynamics approach (**Figure S4A-B**). Parameters for the EXT *O*-glycosylated form were developed in
214 this work and we were able to simulate the EXT *O*-glycosylated system (**Figure S5**). The EXT
215 molecules were modeled in two different states: as a non-glycosylated trimeric helical conformation
216 similar to animal collagen as performed before (Velasquez et al., 2015a) and in the fully *O*-
217 glycosylated state. In addition, we generated molecular dynamics simulations restraining both ends
218 of the polypeptide chains, to model a fully extended helix (consistent with an "indefinitely long
219 EXT"), and without that restriction, to evaluate the conformation that an isolated 10 repeats triple
220 helix would adopt. The results obtained in these simulations indicate the importance of the triple
221 helix conformation in the overall protein stability and especially the conservation of the fibril-like
222 structure, in agreement with 10 repeat single helix simulations performed previously (Marzol et al.
223 2018). Total volume of the extended 10 repeats triple helix was measured in both glycosylation
224 states (**Table 1**), differentiating EXT-protein + *O*-glycans and EXT-protein-only volumes for the fully

225 *O*-glycosylated EXT state. We observe that EXT-protein-only volume is significantly augmented by
226 the presence of the oligosaccharide moieties, indicating that *O*-glycans increase the separation
227 between peptide chains in the EXT triple helix. We also report average diameter for those systems,
228 which are consistent with previously reported atomic force microscopy images (Cannon et al. 2008).
229 Additionally, *O*-glycosylation contributes to increase the average distance between the side chains
230 of tyrosine residues, decreasing the population of tyrosine side chains in close proximity that could
231 lead to cross-linked EXT chains (**Figure S4C**). Current experimental and modeling lines of evidence
232 are in agreement with the proposed role of the proline-hydroxylation and carbohydrate moieties in
233 keeping the EXT molecule in an extended helical polyproline-II conformation state (Stafstrom &
234 Staehelin 1986; Owen et al., 2010; Ishiwata et al., 2014). This extended conformation might allow
235 EXTs to interact properly with themselves and with the surrounding apoplast environment, including
236 PRXs and pectins, to form a proper cell wall network (Nuñez et al., 2009; Valentin et al., 2010).
237
238 To test if the three identified PRXs (PRX01, PRX44 and PRX73) might be able to interact directly with
239 single chain of EXTs, an analysis by homology modeling with a known EXT-PRX GvP1 (from *Vitis*
240 *vinífera*) that is able to crosslink EXTs *in vitro*, was performed (Jackson et al., 2001; Pereira et al.
241 2011). As additional controls, we selected PRX64 described as necessary for the lignin
242 polymerization of capsarian strips in the *Arabidopsis* root endodermis (Lee et al.2013) and PRX36
243 able to bind homogalacturonan pectin in the outer seed coat layer(Francoz et al. 2019). By *docking*
244 analysis, the interaction energy (Kcal/mol) obtained with the three PRXs (PRX01, PRX44, and PRX73)
245 was compared to EXT-PRX GvP1 and with PRX64/PRX36 using 4 different short EXT peptides. A non-
246 hydroxylated EXT peptide $(SPPPYVY)_3$, a hydroxylated but not *O*-glycosylated EXT peptide
247 [$(SOOOYVY)_3$; O=hydroxyproline], only arabinosylated EXT-peptide [$(SOOOYVY)_3$-A] and arabino-
248 galactosylated EXT peptide [$(SOOOYVY)_3$-AG] were analyzed. Previously, it was shown that mutants
249 carrying under-*O*-glycosylated EXTs have severe defect in root hair growth (Velasquez et al. 2011;
250 Velasquez et al. 2015a), and at least for PROLYL 4-HYDROXYLASE 5 mutant (*p4h5*), a modified cell
251 wall structure in the root hair tip was detected (Velasquez et al. 2015b). Docking results for different
252 PRXs tested with various degrees of *O*-glycosylation on EXT peptides show a consistent interaction
253 energy difference depending on the glycosylation state, being higher for non-*O*-glycosylated species
254 (both as proline or hydroxyproline). In addition, EXT *O*-glycosylated variants dock in a rather
255 disperse way while those non-*O*-glycosylated do preferentially in a groove area (**Figure 4A-C**).
256 Furthermore, in **Figure 4A** it is shown how a non-*O*-glycosylated peptide binds through a groove
257 leaving one tyrosine docked in a cavity open to the solvent and very close to the heme iron (5Å),
258 with a second tyrosine a few Angstroms away. This disposition and distances suggest that this could
259 be an active site where the Tyr cross-linking takes place. This statement is reinforced by the fact that
260 almost every substrate docked to the protein (even variably *O*-glycosylated peptides) bind to this
261 pocket. Direct comparison of interaction energies derived from docking experiments with different
262 species would not be rigorous due to the different size and degree of freedom (depending on the *O*-

263 glycosylation) among docking runs (**Figure 4B**). Despite of the fine values, a trend can be observed in
264 **Figure 4C**. When interaction energies are compared among different PRXs interacting with EXT-
265 substrates with the same degree of *O*-glycosylation, it is observed that interaction follows this
266 decreasing order PRX73>PRX01>PRX44 for the non-hydroxylated (Ser-Pro-Pro-Pro) substrate while
267 PRX44>PRX73>PRX01 for the hydroxylated, non-*O*-glycosylatied variant (Ser-Hyp-Hyp-Hyp). In
268 general, it is observed a higher interaction energy (more negative values) for hydroxylated species,
269 followed by non-hydroxylated, and then by *O*-glycosylated variants. Among the non-hydroxylated
270 species, the protein displaying relatively higher interaction energy is PRX73. Among the *O*-
271 glycosylated species, the protein displaying relatively higher interaction energy is PRX44. All
272 together, these results are consistent with a constitutive root hair growth effect for $PRX44^{OE}$ and
273 $PRX73^{OE}$ and also with the non-glycosylated species being the substrates of peroxidation. Overall,
274 this may indicate that PRX44 and PRX73 might interact with EXT substrates, and possibly catalyze
275 Tyr-crosslinking in open regions of the EXT backbones that are naked or with low levels of *O*-glycans.
276 This is in agreement with previous findings suggesting that high levels of *O*-glycosylation in certain
277 EXT segments were found to physically restrict the EXT lateral alignments, possibly by acting as a
278 branching point (Velasquez et al., 2015a). Overall, taking together all the approaches used in this
279 study, these results show that PRX01, PRX44 and PRX73 might be able to crosslink EXTs at Tyr-sites.
280
281 To examine the evolution of these PRXs, PRX01, PRX44, and PRX73, we performed comprehensive
282 phylogenetic analyses of class-III peroxidases across diverse organisms from land plant lineages.
283 Under low selective pressure to maintain substrate specificity, EXT-PRXs activities might have
284 evolved multiple times in parallel during land plant evolution through gene duplication followed by
285 neofunctionalization or subfunctionalization. PRX01, PRX44, and PRX73 belonged to three
286 independent orthologous groups (**Figure S6**) and orthologs genes for each *A. thaliana* PRX have
287 been detected in available Brassicaceae genomes and in various Angiosperms and Gymnosperms
288 families but they were missing from Lycophytes and from non-vascular land plants. It means that
289 these three PRX sequences were the result of ancestral duplications before the divergence between
290 Gymnosperms and Angiosperms but after the emergence of the Tracheophytes (**Figure S6**). Then,
291 orthologs of the three PRX genes have only been detected in true-root containing organisms and
292 these three PRXs are expressed in roots and root hairs, as most of the orthologous sequences (when
293 expression data are available) (**Figure S7**). This strongly supports conserved functions in roots
294 among the three independent orthogroups. Except for PRX73 which belonged to a cluster containing
295 the EXT-PRX from tomato (LePRX38), the other 2 PRXs sequences did not cluster with sequences
296 already described as putative EXT-PRXs from the literature such as PRX09 and PRX40 (Jacobowitz et
297 al. 2019). Indeed, the other known EXT-PRXs (mostly by *in vitro* evidences) are not clustered
298 together but are largely distributed in the tree (**Figure S6**). This analysis suggests that plant EXT-PRXs
299 might have evolved several times in parallel during Tracheophytes evolution.
300

301 Based on the results show in this work, we proposed a working model where these three PRXs,
302 PRX01, PRX44, and PRX73 (and possibly others PRXs) might control root hair growth by channelling
303 H_2O_2 consumption into EXT-crosslinking and impacting on cell wall hardening process. In addition,
304 high levels of ROS in the apical zone of the cytoplasm might activate many other processes also
305 related to polar growth (**Figure S8**). On the contrary, when low levels of PRX proteins linked to a
306 reduced peroxidase activity (as in the triple mutant *prx01,44,73* or SHAM-treated roots), high levels
307 of ROS (as H_2O_2) might accumulate in the apoplast triggering through the oxidative cycle a cell wall
308 loosening effect inhibiting cell growth (**Figure S8**). Concomitantly, deficient PRX activity in the
309 apoplast also triggers lower ROS levels in the cytoplasm of growing root hairs impact on root hair
310 growth. It is hypothesized that high levels of apoplastic ROS may inhibit putative PIP-mediated
311 channelling of ROS (as H_2O_2) to the cytoplasm but this remains to be tested in future experiments.
312

313 **Conclusions**

314 Currently, several of the 73 apoplastic class-III PRXs in *Arabidopsis thaliana* have no assigned
315 biological functions. In this work, we have characterized three EXT-PRXs, PRX01, PRX44 and PRX73
316 that are important for root hair growth linked to ROS-homeostasis and EXT-assembly. These PRXs
317 might control Tyr-crosslinking in EXTs and related glycoproteins and modify its secretion and
318 assembly in the nascent tip cell walls. By using modeling and docking approaches, it was possible to
319 measure the interactions of these PRXs with single chain EXT substrates. All these evidences
320 highlight that PRX01, PRX44 and PRX73 are important enzymes in the EXTs assembly during root hair
321 growth. From the evolutionary point of view, all the putative EXT-PRXs (mostly by *in vitro* evidences)
322 do not clustered together in the phylogenetic tree of class-III PRXs suggesting that plant EXT-PRXs
323 might have evolved several times in parallel during Traqueophytes evolution. Interestingly, as a
324 convergent evolutionary extracellular assembly, proline-rich collagen Class-IV similar to the green
325 EXTs linage and related glycoproteins, is also cross-linked by the activity of a specific class of animal
326 heme-peroxidases (named peroxidasin or PXDN) to form insoluble extracellular networks (Vanacore
327 et al. 2009; Bhave et al. 2012). While collagen IV biophysical properties allows the correct
328 development and function of multicellular tissues in all animal phyla (Brown et al. 2017), EXTs
329 assemblies are also key in several processes of plant cell expansion and morphogenesis (Cannon *et*
330 *al.*, 2008; Velasquez et al. 2015b; Marzol et al. 2018). This might imply that cross-linked extracellular
331 matrices based on proline-rich polymers (e.g. collagens and EXTs) have evolved more than once
332 along eukaryotic evolution to provide mechanical support to single and multiple cellular tissues.
333 Further analyses are required in the future to understand how these EXT-PRXs catalyze at the
334 molecular level the Tyr-crosslinks on EXTs and how this assembly process is regulated during polar
335 cell expansion. In this study we characterized changes in ROS homeostasis and EXT-crosslinking
336 although these are two aspects of a much more complex and boarder balance in these fast growing
337 cells.

338 **Experimental Procedures**

339

340 **Plant and growth conditions**. *Arabidopsis thaliana* Columbia-0 (Col-0) was used as the wild Class
341 (Wt) genoClass in all experiments. All mutants and transgenic lines tested are in this ecoClass.
342 Seedlings were germinated on agar plates in a Percival incubator at 22°C in a growth room with 16h
343 light/8h dark cycles for 10 days at 140 µmol $m^{-2}s^{-1}$ light intensity. Plants were transferred to soil for
344 growth under the same conditions. For identification of T-DNA knockout lines, genomic DNA was
345 extracted from rosette leaves. Confirmation by PCR of a single and multiple T-DNA insertions in the
346 target PRX genes were performed using an insertion-specific LBb1 or LBb1.3 (for SALK lines) primer
347 in addition to one gene-specific primer. To ensure gene disruptions, PCR was also run using two
348 gene-specific primers, expecting bands corresponding to fragments larger than in WT. We isolated
349 homozygous lines for PRX01 (AT1G05240, *prx01-2*, Salk_103597), PRX44 (AT4G26010, *prx44-2*,
350 Salk_057222) and PRX73 (AT5G67400, *prx73-3*, Salk_009296).

351

352 **SS-TOM and SS-TOM-Long-EXT constructs.** The binary vector pART27136 encoding the secreted
353 tdTomato using the secretory signal sequence from tomato polygalacturonase, under the control of
354 the CaMV 35S promoter, were kind gifts of Dr. Jocelyn Rose, Cornell University (named pART-SS-
355 TOM). The entire reporter protein construct was excised from pART-SS-TOM by digesting with *Not*I.
356 The resulting fragments were gel-purified with the QIAquick Gel Extraction Kit and ligated using T4
357 DNA Ligase (New England Biolabs) into dephosphorylated pBlueScript KS+ that had also been
358 digested with *Not*I and gel-purified to make pBS-SS-TOM. The plasmids were confirmed by
359 sequencing with primers 35S-FP (5'-CCTTCGCAAGACCCTTCCTC-3') and OCS-RP (5'-
360 CGTGCACAACAGAATTGAAAGC-3'). The Long-EXT domain sequences from *SlPEX1* (NCBI accession
361 AF159296128) was then removed from pUC57-high and subcloned into pUC57-less by digestion of
362 both pUC57-high and pUC57-less with *Pst*I and *Nsi*I followed by gel purification and ligation of the
363 two gel-purified fragments to make pUC57-full length. The plasmid pBS-SS-TOM-Long EXT was made
364 by digestion of pUC57-full length and pBS-SS-TOM with *Nde*I and *SgrA*I, followed by gel purification
365 band from pUC57-full length and the 5545 bp band from pBS-SS-TOM, and ligation of the two gel
366 purified fragments. pBS-SS-TOM-Long-EXT plasmid were confirmed by sequencing. All pBS plasmids
367 were also confirmed by digestion. Binary vectors for plant transformation were made by gel
368 purifying the *Not*I insert fragments from the pBS-sec-tdT-long plasmids and ligating them with
369 pART27-SS-TOM backbone that had been digested with *Not*I, gel purified, and dephosphorylated, to
370 obtain pART27-SS-TOM and pART27-SS-TOM-Long-EXT.

371

372 **Root hair phenoClass**. For quantitative analysis of root hair phenoClasss in *PRX01,44,73* mutants,
373 35S:PRX-GFP lines and Wt Col-0, 200 fully elongated root hairs were measured (n roots= 20-30) from
374 seedlings grown on vertical plates for 10 days. Values are reported as the mean ±SD using the Image

375 J software. Measurements were made after 7 days. Images were captured with an Olympus SZX7
376 Zoom microscope equipped with a Q-Colors digital camera.
377
378 **Confocal imaging.** Root hairs were ratio imaged with the Zeiss LSM 710 laser scanning confocal
379 microscope (Carl Zeiss) using a 40X oil-immersion, 1.2 numerical aperture. EGFP (473–505nm)
380 emission was collected using a 458-nm primary dichroic mirror and the Meta-detector of the
381 microscope. Bright-field images were acquired simultaneously using the transmission detector of
382 the microscope. For time-lapse analysis, images were collected every 3 s. Image sequences were
383 analyzed using the Template Matching and Slice Alignment plug-in for ImageJ. Fluorescence
384 intensity was measured in 7 µm ROI at the root hair apex.
385
386 **Peroxidase activity**. Soluble proteins were extracted from roots grown on vertical plates for 10 days
387 by grinding in 20mM HEPES, pH 7.0, containing 1 mM EGTA, 10mM ascorbic acid, and PVP
388 PolyclarAT (100mg g^{-1} fresh material; Sigma, Buchs, Switzerland). The extract was centrifuged twice
389 for 10 min at 10,000 g. Each extract was assayed for protein levels with the Bio-Rad assay (Bio-Rad)
390 and for total peroxidase activity using guaïacol/H_2O_2. Enzyme activity (expressed in nkatal/mg
391 protein) was determined by a guaiacol oxidation-based assay. Values are the mean of three
392 replicates ± SD. P-value of one-way anova, (**) $P<0.001$. PRX activity was measured at 25°C by
393 following the oxidation of 8 mM guaiacol (Fluka) at 470 nm in the presence of 2 mM H_2O_2 (Carlo
394 Erba) in a phosphate buffer (200 mM, pH6.0).
395
396 **Cytoplasmic ROS ($_{cyt}$ROS) measurements in root hairs.** Growth of Arabidopsis seeds on a plate was
397 done with 1% sterile agar for 8 d in a chamber at 22°C with continuous light. These seedlings were
398 incubated in darkness on a slide for 10 min with 50 µM 2′,7′-dichlorodihydrofluorescein diacetate
399 (H_2DCF-DA) at room temperature. Samples were observed with a confocal microscope equipped
400 with a 488-nm argon laser and BA510IF filter sets. A 10× objective was used, 0.30 N.A., 4.7 laser
401 intensity, 1.1 offset, 440 photomultiplier (PMT) (for highest ROS levels), 480 PMT (for ROS media),
402 and gain 3. Images were taken scanning XZY with 2 µm between focal planes. Images were analyzed
403 using ImageJ. To measure ROS highest levels, a circular region of interest (ROI) (r = 2.5) was chosen
404 in the zone of the root hair with the highest intensities. To measure ROS mean, the total area of the
405 root hair was taken.
406
407 **Apoplastic ROS ($_{apo}$ROS) measurements in root hairs.** Levels of apoplastic H_2O_2 in root hair cells
408 were measured using a solution of Amplex™ UltraRed Reagent (AUR, Molecular Probes). Briefly,
409 Arabidopsis seedlings were incubated with 50 µM AUR for 20 min in dark conditions. Stained root
410 hair cells were imaged with a Zeiss LSM5 Pascal laser scanning confocal microscope. The
411 fluorescence emission of oxidized AUR in the apoplast of root hair cells was observed between 585

412 and 610 nm using 543 nm argon laser excitation, 40X objective, N/A= 1.2. Quantification of the AUR
413 probing fluorescence signal was restricted to apoplastic spaces at the root hair tip.
414
415 **Phylogenetic analysis.** 73 class-III PRX protein sequences from *A. thaliana*, two putative lignin class-
416 III PRXs from *Zinnia elegans* and 4 putative Extensin class-III PRXs from *Lupinus album*, *Lycopersicum*
417 *esculentum*, *Phaseolus vulgaris* and *Vitis vinifera*, have been aligned with ClustalW and the tree
418 constructed using the Neighbor-Joining method (Saitou and Nei, 1987). The analyses were
419 conducted in MEGA7 (Kumar, 2016). All protein sequences are available using their ID number
420 (http://peroxibase.toulouse.inra.fr (Savelli et al., 2019).
421
422 **Co-expression analysis network**. Co-expression networks for *RSL4* root hair genes were identified
423 from PlaNet (http://aranet.mpimp-golm.mpg.de) and trimmed to facilitate readability (Mutwill et al.
424 2011). Each co-expression of interest was confirmed independently using the expression angler tool
425 from Botany Array Resource BAR (http://bar.utoronto.ca/ntools/cgi-
426 bin/ntools_expression_angler.cgi) and ATTED-II (http://atted.jp). Only those genes that are
427 connected with genes of interest are included.
428
429 **Tyr-crosslinking analysis.** Root tissues obtained from *PRX01,44,73* mutants, Col-0 and 35S:PRX-GFP
430 lines were hydrolyzed in 6 N HCl (aqueous) with 10 mM phenol (2 mg ml^{-1}; 110 °C; 20 h).
431 Hydrolysates were dried under a steady stream of nitrogen (gas) and then re-dissolved at 10 mg ml^{-1}
432 in water. The hydrolysates were fractionated by gel permeation chromatography on a
433 polyhydroxyethyl A column (inner diameter, 9.4 x 200 mm, 10 nm pore size, Poly LC Inc., Columbia,
434 MD) equilibrated in 50 mM formic acid and eluted isocratically at a flow rate of 0.8 ml min^{-1}. UV
435 absorbance was monitored at 280 nm. Phenylisothiocyanate derivatives of IDT were quantified in
436 hydrolysates after fractionation by gel permeation chromatography. The amounts of Tyr and IDT in
437 the hydrolysates were determined by comparison with authentic Tyr and IDT standards. Response
438 factors were determined from three level calibrations with the Tyr and IDT standards.
439
440 **Western-Blot Analysis**. Plant material (100 mg of root from 15 days old seedlings) was collected in a
441 microfuge tube and ground in liquid nitrogen with 400 mL of protein extracction buffer (125 mM
442 Tris-Cl, pH. 4.4, 2% [w/v] SDS, 10% [v/v] glycerol, 6M UREA, 1% [v/v] b-mercaptoethanol, 1mM
443 PMSF). Samples were immediately transferred to ice. After 4° centrifugation at 13000 rpm for 20
444 minutes, supernatant was move to a new 1.5 ml tube and equal volumes of Laemmli buffer (125
445 mM Tris-Cl, pH. 7.4, 4% [w/v] SDS, 40% [v/v] glycerol, 10% [v/v] b-mercaptoethanol, 0.002% [w/v]
446 bromphenol blue) were added. The samples (0.5–1.0 mg/mL of protein) were boiled for 5 min and
447 30 mL were loaded on 10% SDS-PAGE. The proteins were separated by electrophoresis and
448 transferred to nitrocellulose membranes. Anti-GFP mouse IgG (clones 7.1 and 13.1; Roche Applied
449 Science) was used at a dilution of 1:2,000 and it was visualized by incubation with goat anti-mouse

450 IgG secondary antibodies conjugated to horseradish peroxidase (1:2,000) followed by a
451 chemiluminescence reaction (Clarity Western ECL Substrate; Bio-rad).

452 **Transmission electron microscopy of root hair cell walls.** Seeds were germinated on 0.2x MS, 1%
453 sucrose, 0.8% agar. Seven days after germination, seedlings were transferred to new 0.2x MS, 1%
454 sucrose, 0.8% agar plates with or without 100 µM SHAM. After 4 additional days, 1-mm root
455 segments with root hairs were fix in 2% glutaraldehyde in 0.1M cacodylate buffer pH7.4. Samples
456 were rinsed in cacodylate buffer and post-fixed in 2% OsO4. After dehydration in ethanol and
457 acetone, samples were infiltrated in Epon resin (Ted Pella, Redding, CA). Polymerization was
458 performed at 60°C. Sections were stained with 2% uranyl acetate in 70% methanol followed by
459 Reynold's lead citrate (2.6% lead nitrate and 3.5% sodium citrate [pH 12.0]) and observed in a Tecnai
460 12 electron microscope. Quantitative analysis of cell wall thickness was performed using FIJI.
461

462 **Modeling and molecular docking between PRXs and EXTs.** Modeling and molecular docking: cDNA
463 sequences of PRXs were retrieved from TAIR (PRX01: AT1G05240, PRX36: AT3G50990, PRX44:
464 AT4G26010, PRX64: AT5G42180, PRX73: AT5G67400) and NCBI Nucleotide DB (PRX24Gv:Vitis
465 vinifera peroxidase 24, LOC100254434). Homology modeling was performed for all PRXs using
466 modeller 9.14 (Sali et al. 1993), using the crystal structures 1PA2, 3HDL, 1QO4 and 1HCH as
467 templates, available at the protein data bank. 100 structures where generated for each protein and
468 the best scoring one (according to DOPE score) was picked. The *receptor* for the docking runs was
469 generated by the prepare_receptor4 script from autodock suite, adding hydrogens and constructing
470 bonds. Peptides based on the sequence PYYSPSPKVYYPPPSSYVYPPPPS were used, replacing proline
471 by hydroxyproline, and/or adding *O*-Hyp glycosylation with up to four arabinoses per hydroxyproline
472 in the fully glycosylated peptide and a galactose on the serine, as it is usual in plant *O*-Hyp
473 https://www.ncbi.nlm.nih.gov/pmc/articles/PMC5045529/. Ligand starting structure was generated
474 as the most stable structure by molecular dynamics by Hugo Verli (Velasquez et al. 2015a). All ligand
475 bonds were set to be able to rotate. Docking was performed in two steps, using Autodock vina (Trott
476 et al. 2010). First, an exploratory search over the whole protein surface (exhaustiveness 4) was
477 done, followed by a more exhaustive one (exhaustiveness 8), reducing the search space to a
478 75x75x75 box centered over the most frequent binding site found in the former run.
479

480 **EXT conformational coarse-grained model.** The use of coarse-grained (CG) molecular dynamics
481 (MD) allowed collection of long timescale trajectories. System reduction is significant when
482 compared to all atom models, approximately reducing on order of magnitude in particle number. In
483 addition, a longer integration time step can be used. Protein residues and coarse grained solvent
484 parameters correspond to the SIRAH model (Darre et al. 2014), while ad hoc specific glycan
485 parameters were developed (**Figure S5**). The CG force field parameters developed correspond to
486 arabinofuranose and galactopyranose. Triple helix systems were simulated both, in the non-

487 glycosylated and fully *O*-glycosylated states, where all the hydroxyprolines are bound to a
488 tetrasaccharide of arabinofuranoses, and specific serine residues contain one galactopyranose
489 molecule. They were immersed in WT4 GC solvent box that was constructed to be 2 nm apart from
490 the extensin fiber, and periodic boundary conditions were employed. Coarse grained ions were also
491 included to achieve electroneutrality and 0.15 M ionic strength. All simulations were performed
492 using the GROMACS MD package at constant temperature and pressure, using the Berendsen
493 thermostat (respectively) and Parrinello-Rahman barostat (Parrinello and Rahman 1981), and a 10 fs
494 time step. The obtained trajectories were analysed using the Mdtraj python package (McGibbon et
495 al, 2015) and visualized with Visual Molecular Dynamics (VMD) 1.9.1 (Humphrey et al. 1996).
496 Volume measurements were performed using a Convex Hull algorithm implemented in NumPy
497 (Oliphant 2006), and average diameter calculations were derived from this quantity using simple
498 geometric arguments.

Acknowledgements

We would like to thank to Andres Rossi from the microscopy facility of FIL for his assistance. We thank ABRC (Ohio State University) for providing T-DNA lines seed lines. J.M.E. is Principal Investigator of the National Research Council (CONICET) from Argentina. This work was supported by grants from ANPCyT (PICT2016-0132 and PICT2017-0066) and ICGEB CRP/ARG16-03 and a grant from ICGEB CRP/ARG16-03 and ANPCyT (PICT2016-0132 and PICT2017-0066) to J.M.E. In addition, this research is also funded by Instituto Milenio iBio – Iniciativa Científica Milenio, MINECON to J.M.E. and NSF MCB grant 1614965 to M.S.O.

Author Contribution

E.M and C.B performed most of the experiments and analysed the data. P.R. and C.D. analysed the peroxidase activity and performed phylogenetic analysis. M.H. analysed the Tyr-crosslinking on EXTs. A.A. and A.D.N performed the docking experiments and analysed this data. M.B. and L.C. perform the EXT modelling and analysed this data. M.F. and P.B generated the EXT reporter lines and performed the western blots. J.M.P., D.R.R.M., Y.R., S.M., and F.B.H. analysed the data. J.P., J.P-V., and M.S.O. performed the transmission electron microscopy analysis. J.M.E. designed research, analysed the data, supervised the project, and wrote the paper. All authors commented on the results and the manuscript. This manuscript has not been published and is not under consideration for publication elsewhere. All the authors have read the manuscript and have approved this submission.

Competing financial interest

The authors declare no competing financial interests. Correspondence and requests for materials should be addressed to J.M.E. (Email: jestevez@leloir.org.ar / jose.estevez@unab.cl).

523 **REFERENCES**

524 Abraham, M.J., Murtola, T., Schulz, R., Páll S., Smith, J.C., Hess, B., and Lindahl E. (2015). GROMACS:
525 High performance molecular simulations through multi-level parallelism from laptops to
526 supercomputers. *Software X*, 1–2,19-25. ISSN 2352-7110.

527 Baumberger N, Ringli C, Keller B. (2001). The chimeric leucine rich repeat/extensin cell wall protein
528 LRX1 is required for root hair morphogenesis in *Arabidopsis thaliana*. *Genes & Development* 15,
529 1128–1139.

530 Baumberger N, Steiner M, Ryser U, Keller B, Ringli C. (2003). Synergistic interaction of the two
531 paralogous Arabidopsis genes LRX1 and LRX2 in cell wall formation during root hair
532 development. *Plant J.* 35, 71–81.

533 Berardini T.Z., Reiser L., Li D., Mezheritsky Y., Muller R., Strait E., Huala E. (2015). The arabidopsis
534 information resource: making and mining the "gold standard" annotated reference plant
535 genome. *Genesis* 53(8):474–485.

536 Berendsen, H. J. C., Postma, J.P.M., van Gunsteren, W.F., DiNola, A., and Haak, J.R. (1984) Molecular
537 dynamics with coupling to an external bath. *J. Chem. Phys.* 81, 3684. doi: 10.1063/1.448118.

538 Berman HM, John Westbrook, Zukang Feng, Gary Gilliland, Talapady N Bhat, Helge Weissig, Ilya N
539 Shindyalov, and Philip E Bourne. The protein data bank. *Nucleic Acids Research*, 28(1):235–242,
540 2000.

541 Bernards, M.A., Fleming, W.D., Llewellyn, D.B., Priefer, R., Yang, X., Sabatino, A., and Plourde, G.L.
542 (1999). Biochemical characterization of the suberization-associated anionic peroxidase of
543 potato. *Plant Physiol.* 121: 135–146.

544 Bhave G, Cummings CF, Vanacore RM, Kumagai-Cresse C, Ero-Tolliver IA, Rafi M, Kang J-S,
545 Pedchenko V, Fessler LI, Fessler JH, Hudson BG (2012) Peroxidasin forms sulfilimine chemical
546 bonds using hypohalous acids in tissue genesis. Nat Chem Biol 8:784–790.

547 Brady, J.D., Sadler, I.H., and Fry, S.C. (1996). Di-isodityrosine, a novel tetrametric derivative of
548 tyrosine in plant cell wall proteins: a new potential cross-link. *Biochem. J* 315: 323–327.

549 BrownK.L, C.F. Cummings, R.M. Vanacore and B.G. Hudson. (2017). Building collagen IV smart
550 scaffolds on the outside of cells. *Protein Sci.* 26:2151-2161.

551 Brownleader, M.D., Ahmed, N., Trevan, M., Chaplin, M.F., and Dey, P.M. (1995). Purification and
552 Partial Characterization of Tomato Extensin Peroxidase. *Plant Physiol.* 109: 1115–1123

553 Cannon, M.C., Terneus, K., Hall, Q., Tan, L., Wang, Y., Wegenhart, B.L., Chen, L., Lamport, D.T., Chen,
554 Y., and Kieliszewski, M.J. (2008). Self-assembly of the plant cell wall requires an extensin
555 scaffold. *Proc. Natl. Acad. Sci. USA.* 105: 2226–2231.

556 Case, D.A., Cerutti. D.S., Cheatham, T.E.III., Darden, T.A., Duke, R.E., Giese, T.J., Gohlke, H., Goetz,
557 A.W., Greene, D., Homeyer, N., et al. (2017), AMBER 2017, University of California, San
558 Francisco.

559 Cosio C. & Dunand C. (2009). Specific functions of individual classIII peroxidases genes. *J. Exp. Bot.*
560 62:391–408.

561 Cosio C., Ranocha Ph., Francoz E., Burlat V., Zheng Y., Perry S.E., Ripoll J.-J., Yanofsky M., Dunand C.
562 (2017) The class III peroxidase PRX017 is a direct target of the MADS-box transcription factor 1
563 AGL15 and participates in lignified tissue formation. *New Phytol*. 213: 250-263.

564 Darré, L., Machado, M.R., Brandner, A.F., González, H.C., Ferreira, S., and Pantano, S. (2015). SIRAH:
565 A Structurally Unbiased Coarse-Grained Force Field for Proteins with Aqueous Solvation and
566 Long-Range Electrostatics. *J. Chem. Theory Comput.* 11(2):723–739
567 Darré, L., Tek, A., Baaden, M., and Pantano, S. (2012). Mixing atomistic and coarse grain solvation
568 models for MD simulations: let WT4 handle the bulk. *J. Chem. Theory Comput.* 8:3880–3894.
569 Dong, W., Kieliszewski, M., and Held, M.A. (2015). Identification of the pI 4.6 extensin peroxidase
570 from *Lycopersicon esculentum* using proteomics and reverse-genomics. *Phytochem.* 112:151–
571 159.
572 Dunand, C., Crevecoeur, M., and Penel, C. (2007). Distribution of superoxide and hydrogen peroxide
573 in Arabidopsis root and their influence on root development: possible interaction with
574 peroxidases. *New Phytol*. 174:332–341.
575 Fabrice, T., Vogler, H., Draeger, C., Munglani, G., Gupta, S., Herger, A.G., Knox, P., Grossniklaus, U.,
576 and Ringli, C. (2018). LRX proteins play a crucial role in pollen grain and pollen tube cell wall
577 development. Plant Physiol. 176, 1981–1992.
578 Francoz et al. (2019) Pectin demethylesterification generates platforms that anchor peroxidases to
579 remodel plant cell wall domains. *Developmental Cell* 48, 1-16.
580 Fry, S.C. (1982). Isodityrosine, a new cross-linking amino acid from plant cell-wall glycoprotein.
581 *Biochem. J* 204: 449–455.
582 Hall, Q. and Cannon, M.C. (2002). The cell wall hydroxyproline-rich glycoprotein RSH is essential for
583 normal embryo development in Arabidopsis. *Plant Cell* 14: 1161–1172.
584 Humphrey, W., Dalke, A., and Schulten, K. (1996). VMD: Visual molecular dynamics. *J. Molec.*
585 *Graphics* 14:33-38
586 Jackson, P.A., Galinha, C.I., Pereira, C.S., Fortunato, A., Soares, N.C., Amâncio, S.B., and Pinto
587 Ricardo, C.P. (2001). Rapid deposition of extensin during the elicitation of grapevine callus
588 cultures is specifically catalyzed by a 40-kilodalton peroxidase. *Plant Physiol.* 127: 1065–1076.
589 Jacobowitz, J.R, Doyle W.C., and Weng, J-K. (2019). PRX9 and PRX40 are Extensin Peroxidases
590 Essential for Maintaining Tapetum and Microspore Cell Wall Integrity during Arabidopsis Anther
591 Development. *Plant Cell* 31: 848–86.
592 Kim D Pruitt, Tatiana Tatusova, and Donna R Maglott. Ncbi reference sequences (refseq): a curated
593 non-redundant sequence database of genomes, transcripts and proteins. *Nucleic Acids Research*,
594 35(suppl 1):D61–D65, 2006.
595 Kumar, S., Stecher G., Tamura K. (2016) MEGA7: molecular evolutionaary genetic analysis version
596 7.0 for bigger datasets. *Mol. Biol. Evol.* 33(7): 1870-1874.
597 Kunieda, T., Shimada, T., Kondo, M., Nishimura, M., Nishitani, K., and Hara-Nishimura, I. (2013).
598 Spatiotemporal secretion of PEROXIDASE36 is required for seed coat mucilage extrusion in
599 Arabidopsis. *Plant Cell* 25: 1355–1367.
600 Lamport, D.T.A., Kieliszewski, M.J., Chen, Y., and Cannon, M.C. (2011). Role of the extensin
601 superfamily in primary cell wall architecture. *Plant Physiol*. 156: 11–19.
602 Lee, Y., Rubio, M.C., Alassimone, J., and Geldner, N. (2013). A mechanism for localized lignin
603 deposition in the endodermis. *Cell* 153: 402–412.
604 Liszkay, A., van der Zalm, E., and Schopfer, P. (2004). Production of reactive oxygen intermediates
605 (O(2)(.-), H(2)O(2), and (.)OH) by maize roots and their role in wall loosening and elongation
606 growth. *Plant Physiol.* 136: 3114–23.

607 Machado, M.R. and Pantano, S. (2016) SIRAH tools: mapping, backmapping and visualization of
608 coarse-grained models. *Bioinformatics* 32(10):1568–1570
609 Mangano S. *et al.* (2017). The molecular link between auxin and ROS-controlled root hair growth.
610 *Proc. Natl. Acad. Sci. U.S.A*. 114(20):5289-5294.
611 Marzol E, Borassi C, Bringas M, Sede A, Rodríguez Garcia DR, Capece L, Estevez JM. (2018). Filling the
612 Gaps to Solve the Extensin Puzzle. *Mol Plant*. 11(5):645-658.
613 McGibbon R.T, Beauchamp K.A., Harrigan M.P., Klein C., Swails, J.M., Hernández C.X., Schwantes
614 C.R., Wang, L.P., Lane T.J., Pande V.S. (2015) MDTraj: A Modern Open Library for the Analysis of
615 Molecular Dynamics Trajectories. *Biophysical Journal*, 109(8): 1528-1532
616 Menand B, Yi K, Jouannic S, Hoffmann L, Ryan E, Linstead P, Schaefer DG, Dolan L. (2007). An ancient
617 mechanism controls the development of cells with a rooting function in land plants. Science
618 316:1477-1480.
619 Møller, S.R. et al. (2017). Identification and evolution of a plant cell wall specific glycoprotein
620 glycosyl transferase, ExAD. *Sci. Rep.* 7: 45341.
621 Mutwil, M., Klie, S., Tohge, T., Giorgi, F.M., Wilkins, O., Campbell, M.M., Fernie, A.R., Usadel, B.,
622 Nikoloski, Z. and Persson, S. (2011). PlaNet: combined sequence and expression comparisons
623 across plant networks derived from seven species. *Plant Cell*, 23, 895– 910.
624 Oliphant, TE. USA: Trelgol Publishing, (2006). A guide to NumPy. 376 pp.
625 Parrinello, M. and Rahman, A. *(1981).* Polymorphic transitions in single crystals: A new molecular
626 dynamics method. *J. of Applied Physics* 52:7182. doi.org/10.1063/1.328693
627 Passardi, F., Penel, C., and Dunand, C. (2004). Performing the paradoxical: how plant peroxidases
628 modify the cell wall. *Trends Plant Sci*. 9:534–540.
629 Pereira S.P., J.M.L. Ribeiro, A.D. Vatulescu, K. Findlay, A.J. MacDougall and P.A.P. Jackson. (2011)
630 Extensin network formation in *Vitis vinifera* callus cells is an essential and causal event in rapid
631 and H_2O_2-induced reduction in primary cell wall hydration. *BMC Plant Biology* 111:106-121.
632 Price, N.J., Pinheiro, C., Soares, C.M., Ashford, D.A., Ricardo, C.P., and Jackson, P.A. (2003). A
633 biochemical and molecular characterization of LEP1, an extensin peroxidase from lupin. *J. Biol.*
634 *Chem.* 278:41389–41399.
635 Ringli C. (2010). The hydroxyproline-rich glycoprotein domain of the Arabidopsis LRX1 requires Tyr
636 for function but not for insolubilization in the cell wall. *Plant J.* 63, 662–669.
637 Roppolo, D., Boeckmann, B., Pfister, A., Boutet, E., Rubio, M.C., Denervaud-Tendon, V., Vermeer,
638 J.E.M., Gheyselinck, J., Xenarios, I., and Geldner, N. (2014). Functional and evolutionary analysis
639 of the CASPARIAN STRIP MEMBRANE DOMAIN PROTEIN family. Plant Physiol. 165, 1709–1722.
640 Saitou N, Nei M. 1987. The neighbor-joining method: a newmethod for reconstruction of
641 phylogenetic trees. Mol Biol Evol4:406–25.
642 Saito, F., Suyama, A., Oka, T., Yoko-O, T., Matsuoka, K., Jigami, Y., and Shimma, Y.-I. (2014).
643 Identification of Novel Peptidyl Serine α-Galactosyltransferase Gene Family in Plants. *J. Biol.*
644 *Chem.* 289: 20405–20420.
645 Šali A., and Tom L Blundell. Comparative protein modelling by satisfaction of spatial restraints. *J. of*
646 *Molecular biology*, 234(3):779–815, 1993.
647 Savelli B., Li Q., Webber M., Jemmat A.M., Robitaille A., Zamocky M., Mathe C., Dunand C. (2019).
648 RedoxiBase a database for ROS homeostasis regulated proteins. *Redox Biol*.
649 doi.org/10.1016/j.redox.2019.101247.

650 Schnabelrauch, L.S., Kieliszewski, M., Upham, B.L., Alizedeh, H., and Lamport, D. (1996). Isolation of
651 pl 4.6 extensin peroxidase from tomato cell suspension cultures and identification of Val-Tyr-Lys
652 as putative intermolecular cross-link site. *Plant J.* 9:477–489.
653 Sede, A.R., Borassi, C., Wengier, D.L., Mecchia, M.A., Estevez, J.M., and Muschietti, J.P. (2018).
654 Arabidopsis pollen extensins LRX are required for cell wall integrity during pollen tube growth.
655 FEBS Lett. 592, 233–243.
656 Shen Y., Rosendale M., Campbell R.E., D. Perrais (2014). pHuji, apH-sensitive red fluorescent protein
657 for imaging of exo- and endocytosis. *J.Cell Biol.* 207 (3):419-432.
658 Shigeto, J. and Tsutsumi, Y. (2016). Diverse functions and reactions of class III peroxidases. *New*
659 *Phytol*. 209: 1395–1402.
660 Showalter AM, Keppler B, Lichtenberg J, Gu D, Welch LR. 2010. A bioinformatics approach to the
661 identification, classification, and analysis of hydroxyproline-rich glycoproteins. *Plant Physiology*
662 153, 485–513.
663 Smith, A.T., Santama, N., Dacey, S., Edwards, M., Bray, R.C., Thorneley, R.N., and Burke, J.F. (1990).
664 Expression of a synthetic gene for horseradish peroxidase C in *Escherichia coli* and folding and
665 activation of the recombinant enzyme with Ca2+ and heme. *J. Biol. Chem.* 265: 13335–13343.
666 Stoddard, A & Rolland, V. (2018). I see the light!. Fluorescent proteins suitable for the cell
667 wall/apoplat targeeting in *Nicotiana benthamiana* leaves. *Plant Direct.* doi.org/10.1002/pld3.112
668 Tognolli, M., Penel, C., Greppin, H., and Simon, P. (2002). Analysis and expression of the class III
669 peroxidase large gene family in *Arabidopsis thaliana*. *Gene* 288: 129–138.
670 Trott O., and Arthur J Olson. (2010). Autodock vina: improving the speed and accuracy of docking
671 with a new scoring function, efficient optimization, and multithreading. *Journal of*
672 *Computational Chemistry*, 31(2):455–461.
673 Vanacore R, Ham AJ, Voehler M, Sanders CR, Conrads TP, Veenstra TD, Sharpless KB, Dawson PE,
674 Hudson BG (2009) A sulfilimine bond identified in collagen IV. Science 325:1230–1234.
675 Velasquez, S.M., Ricardi, M.M., Dorosz, J.G., Fernandez, P.V., Nadra, A.D., Pol-Fachin, L., Egelund, J.,
676 Gille, S., Ciancia, M., Verli, H., et al. (2011). O-glycosylated cell wall extensins are essential in root
677 hair growth. *Science* 332:1401–1403.
678 Velasquez M, Salter JS, Dorosz JG, Petersen BL, Estevez JM. (2012). Recent advances on the
679 posttranslational modifications of EXTs and their roles in plant cell walls. *Frontiers in plant*
680 *science* 3, 93.
681 Velasquez SM, Marzol E, Borassi C, Pol-Fachin L, Ricardi MM, Mangano S, Denita JS, Salgado SJ,
682 Gloazzo DJ, Marcus SE. (2015a). Low sugar is not always good: Impact of specific O-glycan
683 defects on tip growth in Arabidopsis. *Plant Physiology* 168, 808–813.
684 Velasquez, S.M., Ricardi, M.M., Poulsen, C.P., Oikawa, A., Dilokpimol, A., Halim, A., Mangano, S.,
685 Denita-Juarez, S.P., Marzol, E., Salgoda Salter, J.D., et al. (2015b). Complex regulation of prolyl-4-
686 hydroxylases impacts root hair expansion. *Mol. Plant* 8:734–746.
687 Wang, X., Wang, K., Yin, G., Liu, X., Liu, M., Cao, N., Duan, Y., Gao, H., Wang, W., Ge, W., et al.
688 (2018). Pollen-expressed leucine-rich repeat extensins are essential for pollen germination and
689 growth. Plant Physiol. 176, 1993–2006.
690 Welinder, K.G., Justesen, A.F., Kjaersgard, I.V., Jensen, R.B., Rasmussen, S.K., Jespersen, H.M., and
691 Duroux, L. (2002). Structural diversity and transcription of class III peroxidases from *Arabidopsis*
692 *thaliana*. *Eur. J. Biochem*. 269: 6063–6081.

693 Wojtaszek, P., Trethowan, J., and Bolwell, G.P. (1997). Reconstitution in vitro of the components and
694 conditions required for the oxidative cross-linking of extracellular proteins in French bean
695 (Phaseolus vulgaris L.). *FEBS Lett.* 405:95–98.

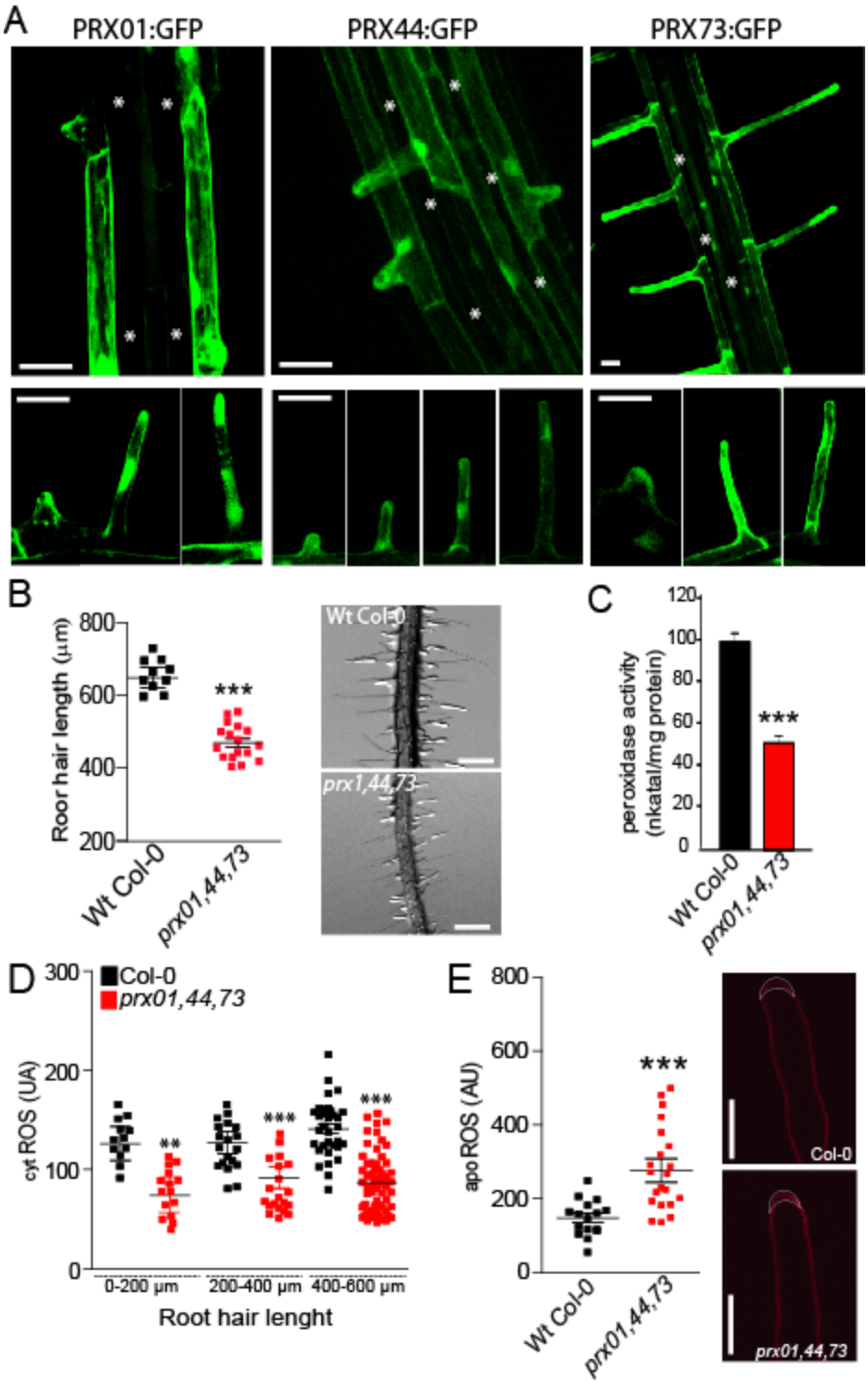

Figure 1. Characterization of root hair specific PRX01, PRX44 and PRX73 expression and mutant analysis.

700 (**A**) Transcriptional reporters of PRX01, PRX44 and PRX73 GFP-tagged in the root elongation zone
701 and specifically in root hairs (bottom). Scale bar = 20 µm. (*) means lack of expression in
702 atrichoblast cell layers.
703 (**B**) Root hair phenoClass of wild-Class (Columbia, Col-0) and *prx01,44,73* triple mutant. Box-plot of
704 root hair length. Horizontal lines show the means. (***) P<0.001 determined by one-way ANOVA.
705 Scale bars, 1 mm.
706 (**C**) Peroxidase activity in wild-Class (Columbia, Col-0) and *prx01,44,73* triple mutant roots. Enzyme
707 activity values (expressed as nkatal/mg protein) are the mean of three replicates ± SD. P-value of
708 one-way anova, (***) P < 0.001.
709 (**D**) Cytoplasmic ROS levels measured with H_2DCF-DA in Wild-Class (Columbia Col-0) and in the triple
710 mutant *prx01,44,73*. P-value of one-way anova, (***) P<0.001 and (**) P<0.01.
711 (**E**) Apoplastic ROS levels measured with Amplex™ UltraRed (AUR) in wild-Class (Columbia Col-0) and
712 in the triple mutant *prx01,44,73*. ROS signal was quantified from the root hair cell tip. P-value of
713 one-way anova, (***) P<0.001. Scale bar= 10 µm.

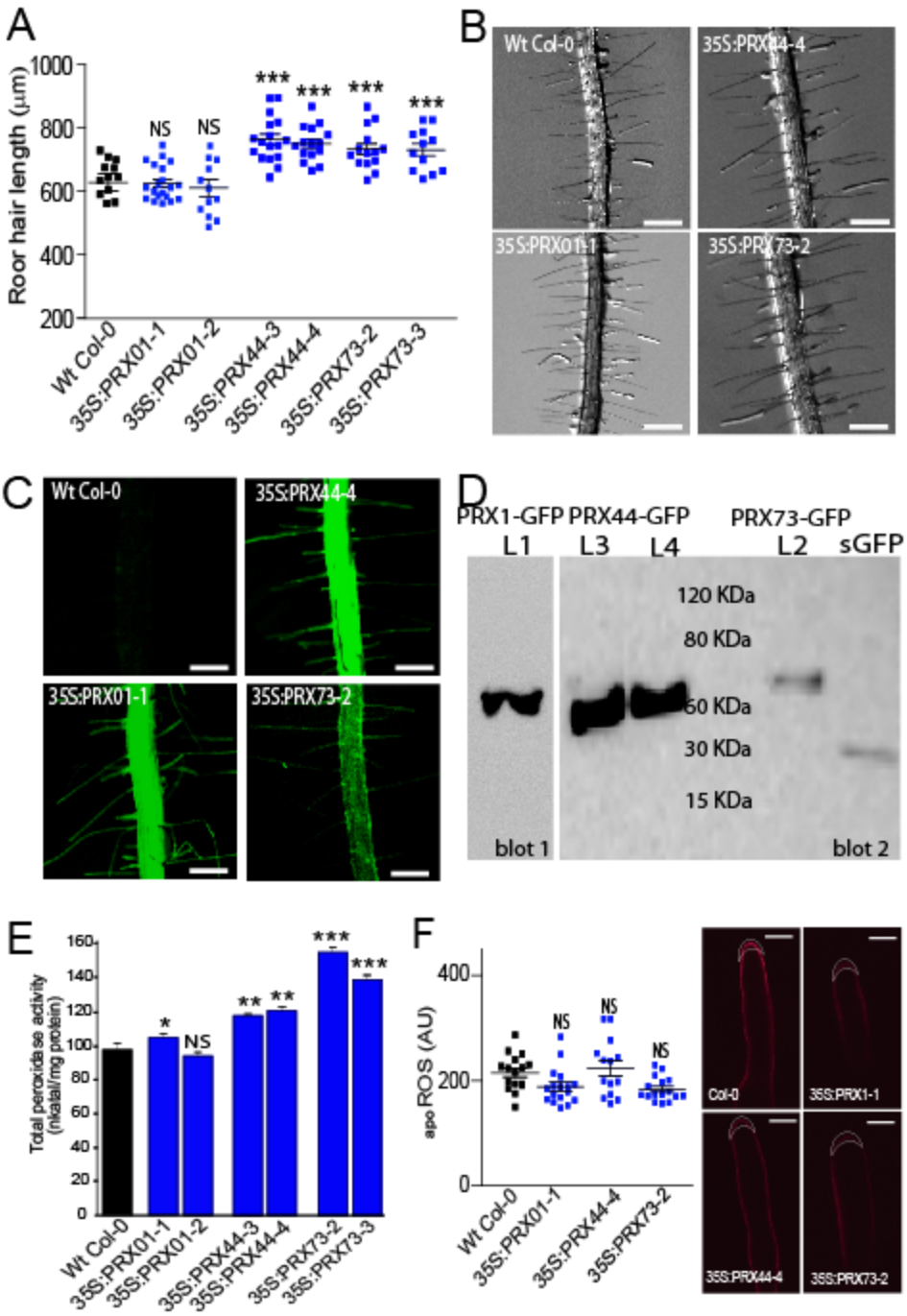

Figure 2. High level of expression of PRX44 and PRX73 trigger ectopic growth linked to higher peroxidase activity.

(**A**) Root hair phenoClass of wild-Class (Columbia, Col-0) and PRXs^{OE} lines (in Wt Col-0). Box-plot of root hair length. Horizontal lines show the means. ** P<0.001 determined by one-way ANOVA. Scale bars, 1 mm. (NS) not significantly different.

(**B**) Selected pictures of root hair phenoClass analyzed in Figure 2A. Scale bar= 0.5mm.

722 (**C**) Expression of GFP-tagged 35S:PRX01, 35S:PRX44 and 35S:PRX73 in root hair cells.
723 (**D**) Western Blot of PRX01-GFP, PRX44-GFP and PRX73-GFP. Soluble GFP (sGFP) was used as control.
724 The predicted molecular weights are 62.6 KDa for PRX01-GFP, 60.8 KDa for PRX44-GFP, 62.9 KDa for
725 PRX73 and 27 KDa for sGFP.
726 (**E**) Assays of total peroxidase activity in wild-Class (Columbia Col-0) and $PRXs^{OE}$ lines (in Wt Col-0).
727 Enzyme activity (expressed in nkatal/mg protein) was determined by a guaiacol oxidation-based
728 assay. Values are the mean of three replicates ± SD. P-value of one-way anova, (***) P<0.001, (**)
729 P<0.01, (*) P<0.1.
730 (**F**) Apoplastic ROS levels measured with Amplex™ UltraRed (AUR) in wild-Class (Columbia Col-0) and
731 $PRXs^{OE}$ lines (in Wt Col-0). ROS signal was quantified from the root hair cell tip. P-value of one-way
732 anova, (NS) not significantly different. Scale bar= 10 µm.

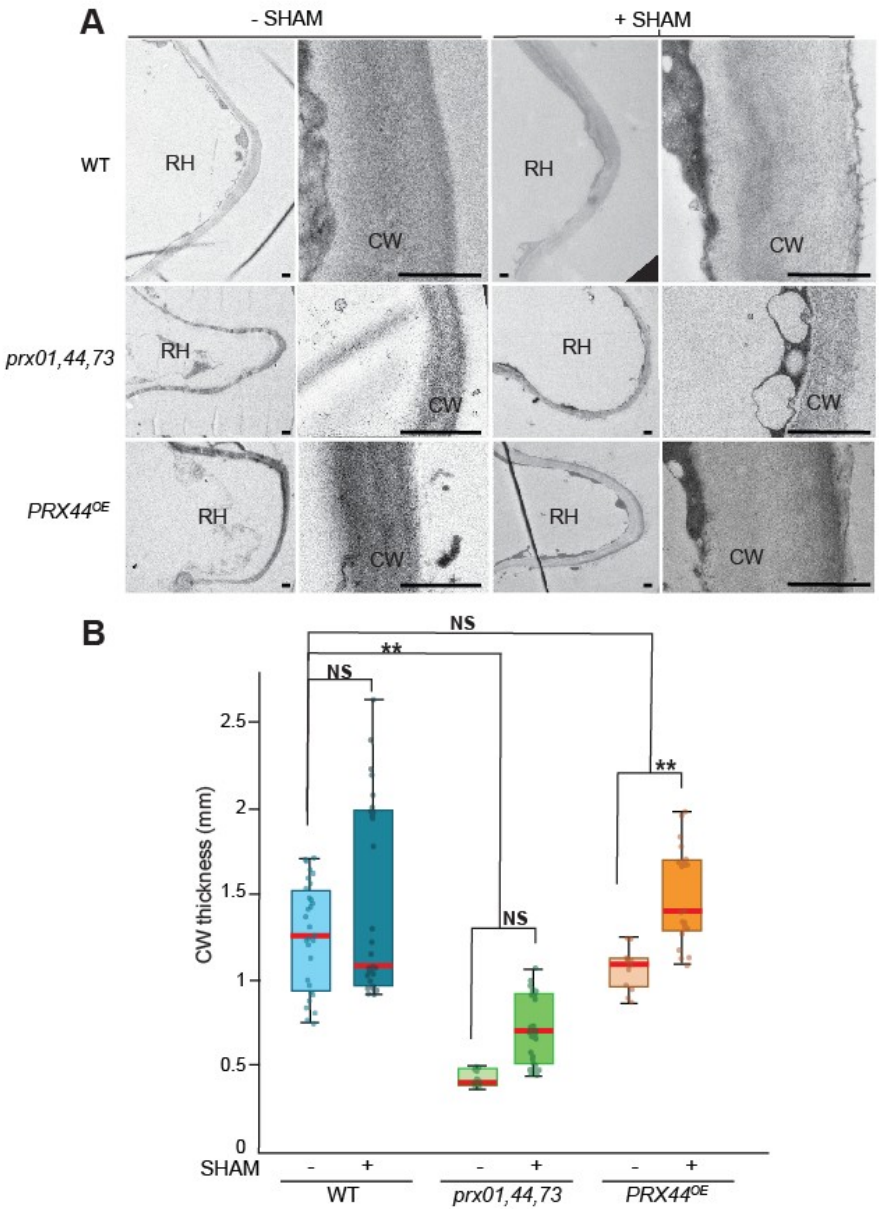

Figure 3. Impact of deficient PRXs on the cell wall thickness in the root hair tips.

(A) Transmission electron micrographs of root hair tips from Wt Col-0, *prx1,44,73* triple mutant, and $PRX44^{OE}$ with (+) and without (-) SHAM. For each genotype and treatment, a representative overview of a root hair (RH) and a detail of the cell wall at the root hair tip (CW) is shown. (B) Whisker plot showing the cell wall thickness at the root hair tip of the three genotypes with or without SHAM treatment. ** P<0.001 determined by one-way ANOVA. (NS) not significantly different. Scale bars = 1µm.

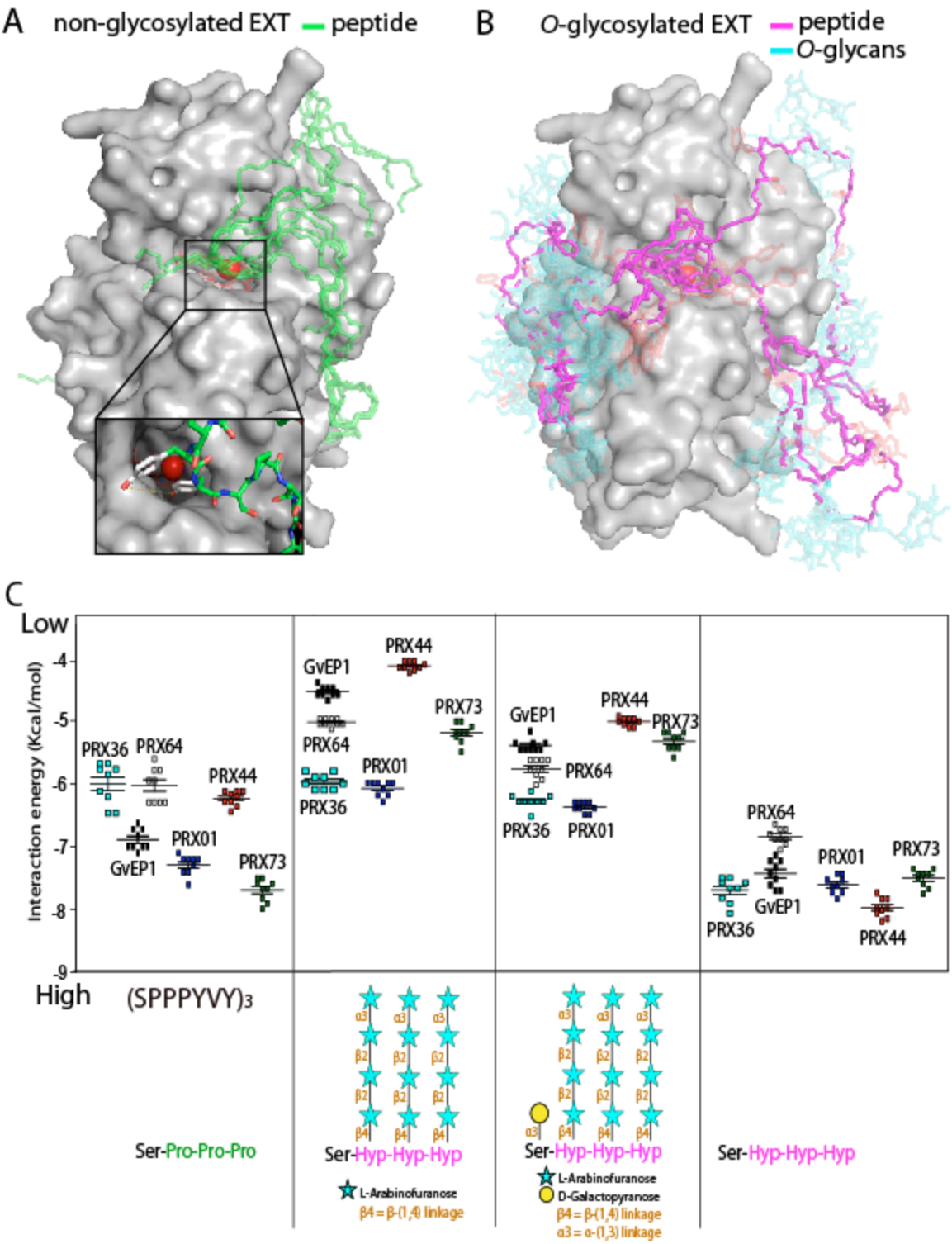

742

743 **Figure 4. Interaction by an *in silico* docking approach of PRX01, PRX44 and PRX73 with EXT**
744 **peptides.**
745 **(A)** PRX44 is shown as a protein surface in gray, with 10 docking results superimposed for each *O*-
746 glycosylation state, to evaluate the consistency of docking sites. Model of a PRX44 complexed to a

747 non-*O*-glycosylated EXT substrate $(SPPPYVY)_3$ (in green). Detail of a non-glycosylated EXT substrate
748 depicted as sticks, docked to the protein represented as surface in gray. Heme is depicted as thin
749 sticks while iron is as a red sphere. On the bottom, two close tyrosine residues dock close to the
750 active site of PRX44.
751 (**B**) Model of a PRX44 complexed to an *O*-glycosylated-EXT substrate (in magenta the protein
752 backbone and in light blue the *O*-Glycans). Detail of an *O*-glycosylated EXT substrate depicted as
753 sticks, docked to the protein represented as surface in gray. Heme is depicted as thin sticks while
754 iron is as a red sphere. Arabino-galactosylated EXT peptide = $[(SOOOYVY)_3$-AG].
755 (**C**) A non-hydroxylated EXT peptide $(SPPPYVY)_3$, a hydroxylated but not *O*-glycosylated EXT peptide
756 $[(SOOOYVY)_3$; O=hydroxyproline], only arabinosylated EXT-peptide $[(SOOOYVY)_3$-A] and arabino-
757 galactosylated EXT peptide $[(SOOOYVY)_3$-AG] were analyzed. Comparison of the binding energy of
758 different peroxidases to its EXT substrates with different degrees of *O*-glycosylation.

759 **Supplementary Materials**
760

761 **PRX01, PRX44, and PRX73 are class-III extensin-related peroxidases that modulates root hair**
762 **growth in *Arabidopsis thaliana***

763
764 Eliana Marzol[1,#], Cecilia Borassi[1,#], Philippe Ranocha[2], Alejandro Aptekman[3,4], Mauro Brindas[5],
765 Janice Pennington[6], Julio Paez-Valencia[6], Javier Martínez Pacheco[1], Diana Rosa Rodríguez Garcia[1],
766 Yossmayer Rondon[1], Mariana Carignani[1], Silvina Mangano[1], Margaret Fleming[7], Francisca Blanco-
767 Herrera[8,9], Patricia Bedinger[7], Christophe Dunand[2], Luciana Capece[5], Alejandro Nadra[3,4], Michael
768 Held[10], Marisa Otegui[6,11] & José M. Estevez[1,8,†]
769
770
771 [#]co-first authors
772 [†] Correspondence should be addressed. Email: jestevez@leloir.org.ar / jose.estevez@unab.cl (J.M.E).

773
774 **Supplementary Materials**
775 Tables S1-S2
776 Supplementary Figures S1-S8

777 **Table S1**. Peptidyl-Tyr and iso-dityrosine (IDT) contents in cell walls isolated from Wt Col-0, PRX^{OE}
778 lines and under *O*-glycosylated EXTs lines. *** P<0.001, ** P<0.01 and * P<0.1 determined by one-
779 way ANOVA. STD=Standard Deviation. In blue higher values and in light blue lower values than Wt
780 Col-0 are highlighted.
781

	ng Tyr/µg CW (STD)	ng IDT/µg CW (STD)
Wt Col-0	7.799 ± 0.26	0.853 ± 0.08
prx01 prx44 prx73	9.588 ± 0.31**	0.963 ± 0.02
PRX44^{OE}	8.649 ± 0.07	0.953 ± 0.04
PRX73^{OE}	8.700 ± 0.12	1.042 ± 0.02*
under O-glycosylated EXTs		
sergt1-1 rra3	3.530 ± 0.08***	0.235 ± 0.01***
p4h5 sergt1-1	3.766 ± 0.06***	0.225 ± 0.02***

782

783

784

785 **Table S2**. Volume and average diameter measurements on EXTs from molecular dynamics
786 simulations. These magnitudes were measured in the fully extended EXT system.
787

	Non-glycosylated EXT	*O*-glycosylated EXT	*O*-glycosylated EXT (protein only)
Volume /nm^3	280 ± 30	1080 ± 50	450 ± 30
EXT length /nm	65 ± 2	70 ± 2	70 ± 2
Average diameter /nm	2.4	4.5	2.9
Distance Tyr-Tyr			
0-5 Å	20%	25%	-
5-7 Å	55%	65%	-

788

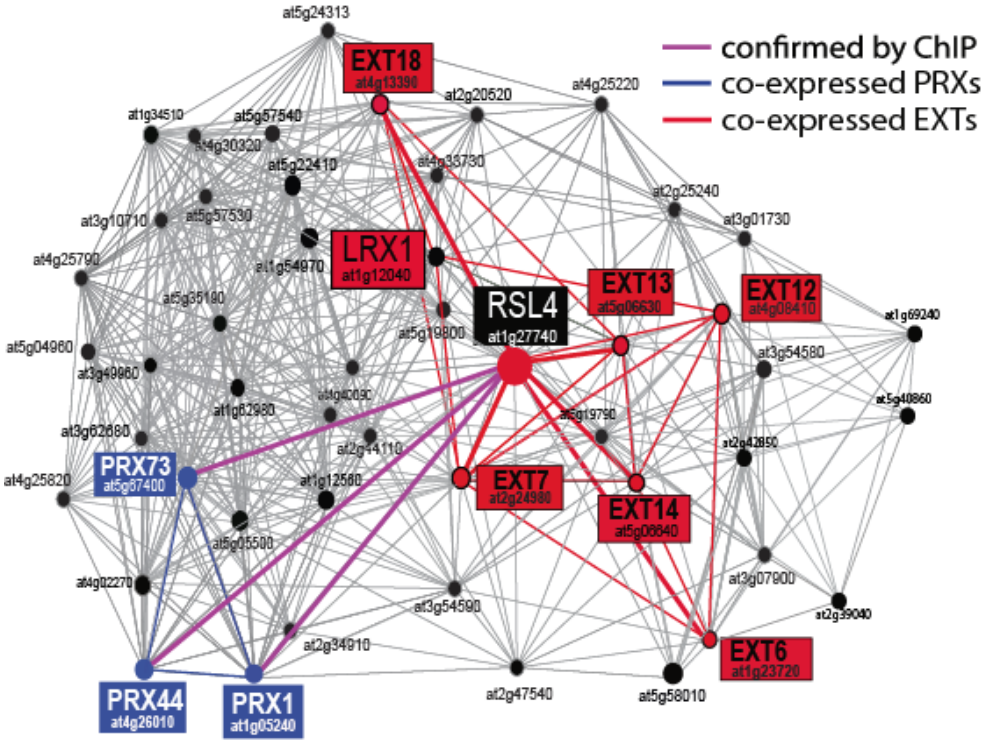

Figure S1. **Root hair transcriptional co-expression network: PRXs, EXTs, and the transcriptional regulator RSL4 are highlighted.** RSL4 was used as gene bait to narrow down the number of co-expressed genes. Transcriptional connections between RSL4 and PRXs genes (in red) and bait genes RSL4 (in black) are highlighted. The co-expression network was identified from PLaNet (http://aranet.mpimp-golm.mpg.de/aranet) (Mutwil et al., 2011) and trimmed to facilitate readability. Chromatin immunoprecipitation assay (ChiP) showed that RSL4 binds and controls the expression of PRX01,44,73 (Mangano et al. 2017).

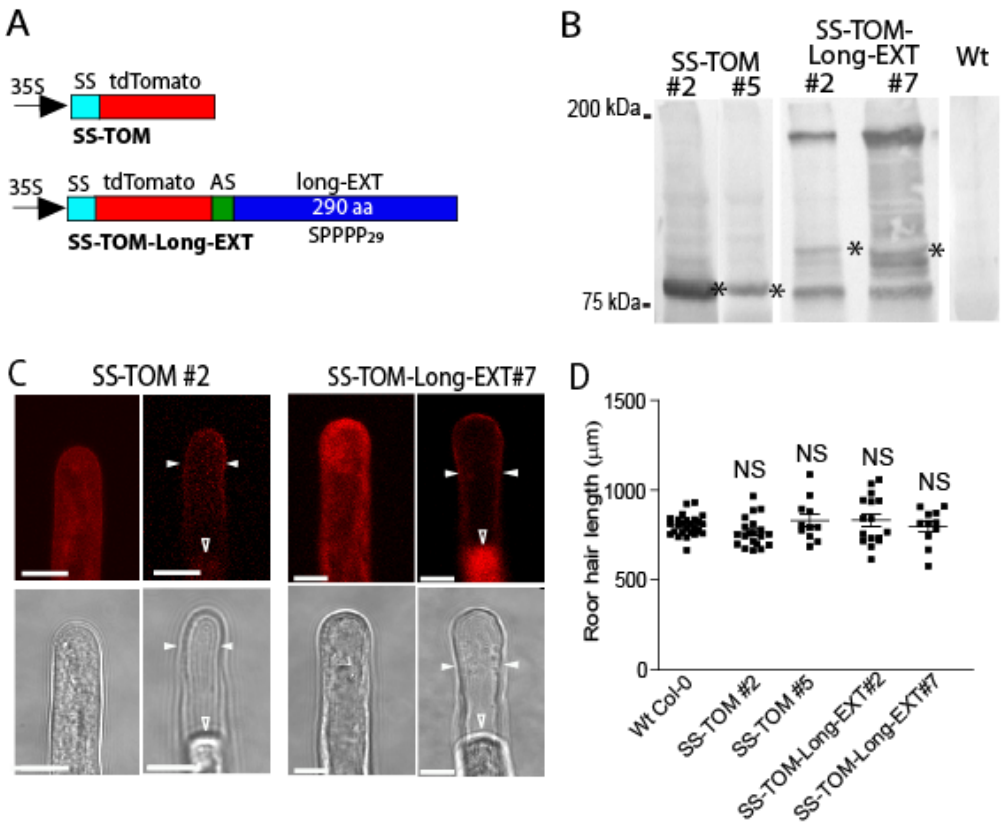

Figure S2. EXT reporter is expressed and targeted to root hair cell walls.

(**A**) Schematic diagrams of SS-TOM and SS-TOM-Long-EXT constructs expressed under the control of the 35S promoter in Arabidopsis plants. SS, Tomato polygalacturonase signal sequence. AS, Ala-spacer, 6 alanines between tdTomato (TOM) and Long-EXT domain. Long-EXT, C-terminal 290 amino acids of *SlPEX1*.

(**B**) Expression and detection of EXT-reporters in homozygous *Arabidopsis* lines. Lines expressing detectable levels of SS-TOM (lines #2 and #5) and SS-TOM-Long-EXT (lines #2 and #7) showed similarly unexpectedly large sizes of protein on the Western blot, with bands much larger than 94 kDa (which is the predicted size of the unmodified EXT protein). All the gel blots shown are part of the same run.

(**C**) Expression of SS-TOM and SS-TOM-Long-EXT reporters in *Arabidopsis* root hair cells. (On the bottom) Bright-field images (On the bottom left) cells were plasmolyzed in 1 M NaCl. Cell wall location is denoted with solid arrowheads while plasma membrane is indicated with an empty arrowhead. Scale bar= 10 µm.

(**D**) Root hair phenoClass of Wild-Class (Columbia, Col-0), SS-TOM (#2 and #5) and SS-TOM-Long-EXT (in Wt Col-0) as box-plot. Horizontal lines show the means. NS= not significant different, determined by one-way ANOVA.

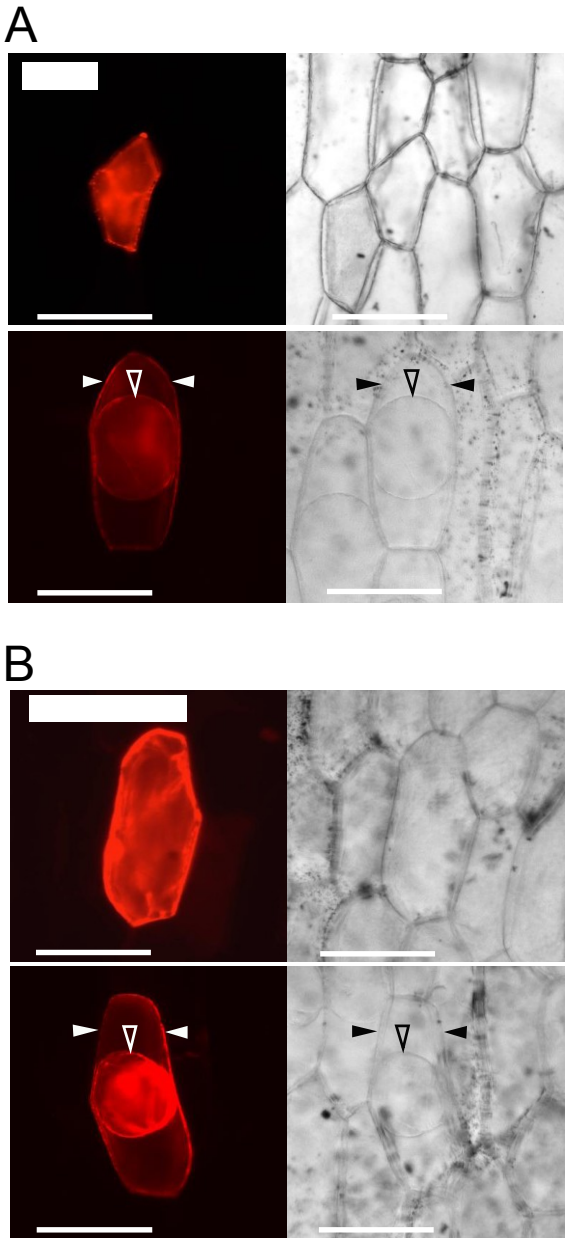

Figure S3. **Expression of EXT-reporter in transiently transformed onion epidermal cells.**
(**A**) Onion epidermis expressing SS-TOM. (On the right) Bright field images. (On the bottom) cells were plasmolyzed in 1 M NaCl. Cell wall location is denoted with solid arrowheads while plasma membrane is indicated with an empty arrowhead. Scale bar= 100 µm. SS=Signal Peptide. TOM=Tomato fluorescent protein.
(**B**) Onion epidermis expressing SS-TOM-Long-EXT. (On the right) Bright fields images. (On the bottom) Cells were plasmolyzed in 1 M NaCl. Cell wall location is denoted with solid arrowheads while plasma membrane is indicated with an empty arrowhead. Scale bar= 100 µm. SS=Signal Peptide. TOM=Tomato fluorescent protein. Long-EXT= C-terminal 290 amino acids of *Solanum lycopersicum* (Sl) *SlPEX1*.

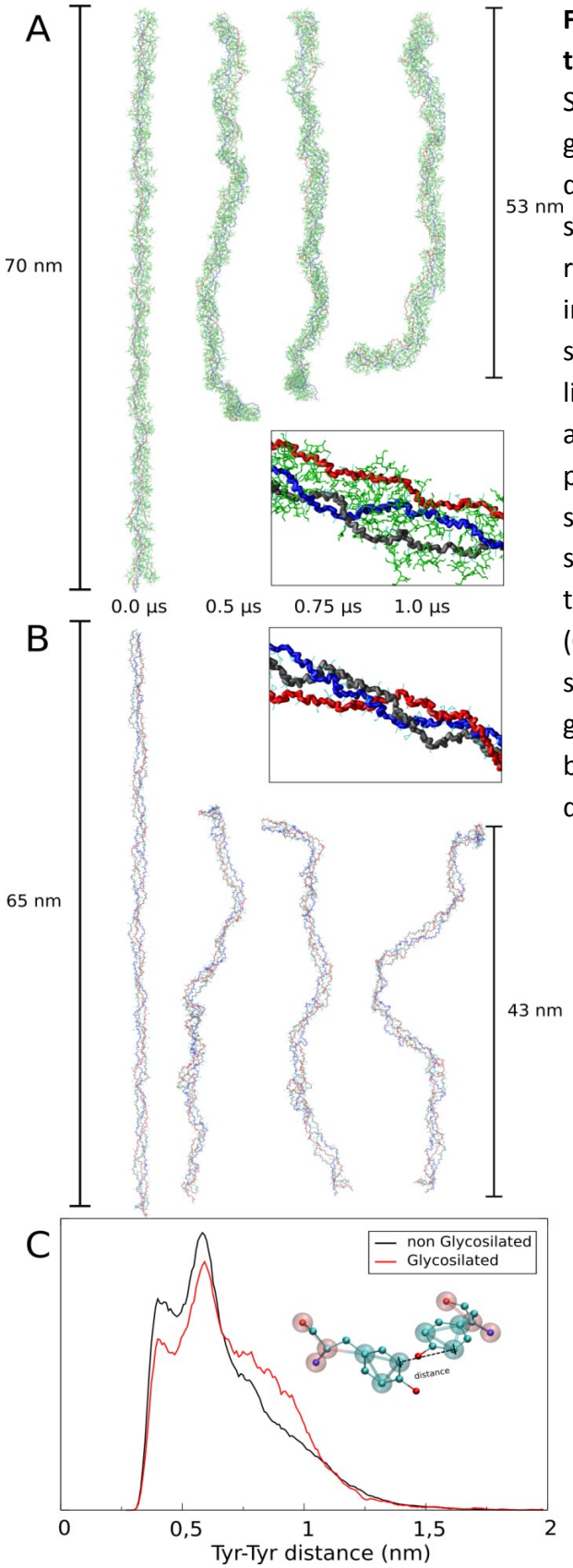

Figure S4. Effect of the *O*-glycosylation status on the triple helix EXT assembly and Tyr-Tyr distances.

Selected snapshots of the O-glycosylated (**A**) and non-glycosylated **(B)** triple EXT chain MD (molecular dynamics) trajectory, showing the stability of the triple strand along 1 us molecular dynamics simulation. The results obtained in these simulations highlight the importance of the triple-helix EXT in overall protein stability, and especially the maintenance of the fibril-like structure. Peptide chains are depicted in red, black and blue and glycans in green. In these simulations the peptide chains are allowed to move freely inside the simulation box, without any restrictions. Insets: a snapshot of a 25-aminoacid portion of the triple helix taken from the CG MD trajectory.

(**C**) Distribution of the Tyr-Tyr distances along the MD simulations for the glycosylated (red line) and non-glycosylated (black line) states. Distances are measured between the C-*ortho* of the Tyrosine residues (as depicted in the inset of the figure).

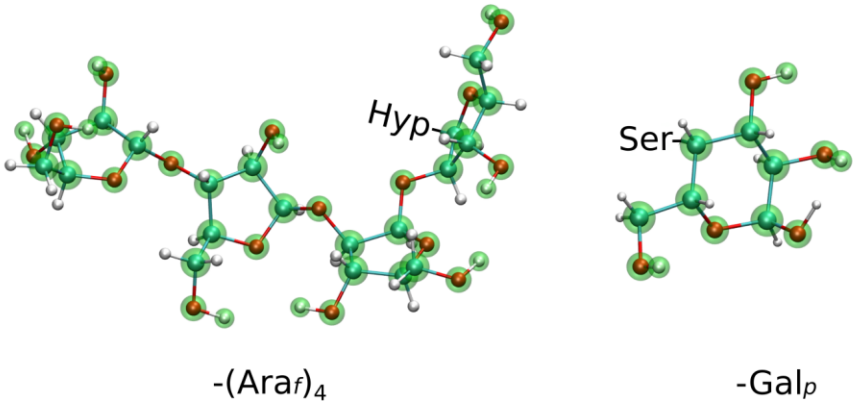

Figure S5. **Coarse-grained models for tetra-arabinofuranose and galactopyranose moieties (diffuse green spheres) superimposed on all atom description (solid spheres connected by tubes)**. Interaction points or beads are located in the position of the heavy atoms and hydrogens corresponding to hydroxyl groups. The latter were included due to the importance of directional hydrogen bond-like interactions in this Class of molecules. Mass and Lennard-Jones parameters of CG beads and spring constants for intramolecular interactions were chosen to be compatible with the SIRAH coarse-grained model (parameters are available upon request).

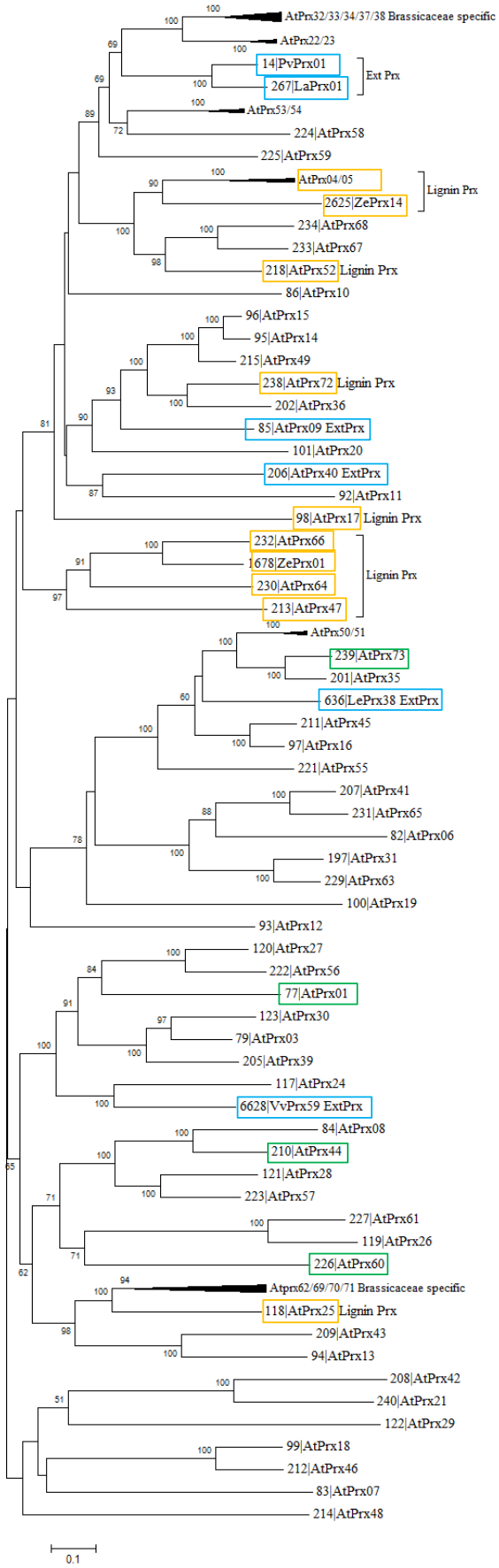
AtPrx32/33/34/37/38 Brassicaceae specific
AtPrx22/23
14|PvPrx01
267|LaPrx01
Ext Prx
AtPrx53/54
224|AtPrx58
225|AtPrx59
AtPrx04/05
2625|ZePrx14
Lignin Prx
234|AtPrx68
233|AtPrx67
218|AtPrx52 Lignin Prx
86|AtPrx10
96|AtPrx15
95|AtPrx14
215|AtPrx49
238|AtPrx72 Lignin Prx
202|AtPrx36
85|AtPrx09 ExtPrx
101|AtPrx20
206|AtPrx40 ExtPrx
92|AtPrx11
98|AtPrx17 Lignin Prx
232|AtPrx66
1678|ZePrx01
230|AtPrx64
213|AtPrx47
Lignin Prx
AtPrx50/51
239|AtPrx73
201|AtPrx35
636|LePrx38 ExtPrx
211|AtPrx45
97|AtPrx16
221|AtPrx55
207|AtPrx41
231|AtPrx65
82|AtPrx06
197|AtPrx31
229|AtPrx63
100|AtPrx19
93|AtPrx12
120|AtPrx27
222|AtPrx56
77|AtPrx01
123|AtPrx30
79|AtPrx03
205|AtPrx39
117|AtPrx24
6628|VvPrx59 ExtPrx
84|AtPrx08
210|AtPrx44
121|AtPrx28
223|AtPrx57
227|AtPrx61
119|AtPrx26
226|AtPrx60
Atprx62/69/70/71 Brassicaceae specific
118|AtPrx25 Lignin Prx
209|AtPrx43
94|AtPrx13
208|AtPrx42
240|AtPrx21
122|AtPrx29
99|AtPrx18
212|AtPrx46
83|AtPrx07
214|AtPrx48
0.1

867

868 **Figure S6. Evolutionary relationships of class-III PRXs with putative EXT cross-linking activity.**
869 The 73 PRXs protein sequences from *A. thaliana*, 2 putative Lignin-PRX from *Zinnia elegans* and 4
870 putative EXT-PRX from *Lupinus album*, *Lycopersicum esculentum*, *Phaseolus vulgaris* and *Vitis*
871 *vinifera*, have been aligned with ClustalW and the tree constructed using the Neighbor-Joining
872 method (Saitou and Nei, 1987). The analysis was conducted in MEGA7 (Kumar, 2016). Previous
873 identified PRXs with putative EXT-PRXs are indicated in blue boxes. The EXT-PRXs studied in the
874 present work are highlighted in green boxes. All protein sequences are available using their ID
875 number (http://peroxibase.toulouse.inra.fr; Savelli et al., 2019).

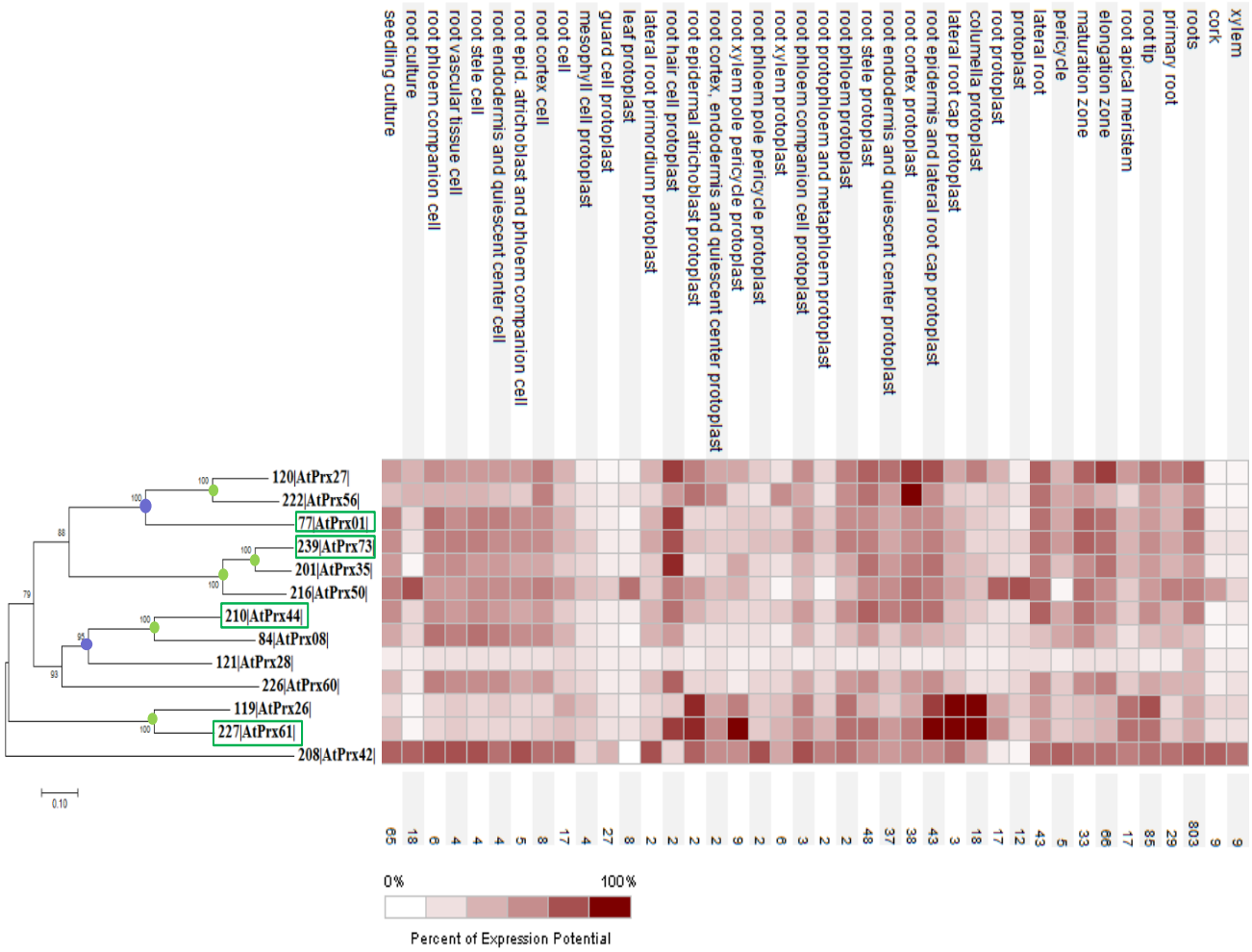

Figure S7. Evolutionary and root tissue expression relationships of putative EXT-PRXs in Arabidopsis.

The evolutionary history of apoplastic class-III PRXs in root hairs associated has been associated to 15 PRXs protein sequences of *A. thaliana*. They have been aligned with ClustalW and the tree constructed using the Neighbor-Joining method (Saitou and Nei, 1987). The analyses were conducted in MEGA7 (Kumar 2016). The sequences of AtPRX01/PRX2 and AtPRX50/51 are either identical or very close, leading to only two independent expression profiles from Affymetrix data. A brown (max value)-to-cream (min value) heat-map was drawn from 105 anatomical parts from data selection available from AT_AFFY_ATH1-0 and plotted in front of each branch and using Genevestigator. The class-III PRXs studied in the present work were surrounded in green. Green and blue circles correspond to duplication posterior to Brassicaceae and to Dicotyledons emergences respectively. All protein sequences are available using their ID number (http://peroxibase.toulouse.inra.fr; Savelli et al., 2019).

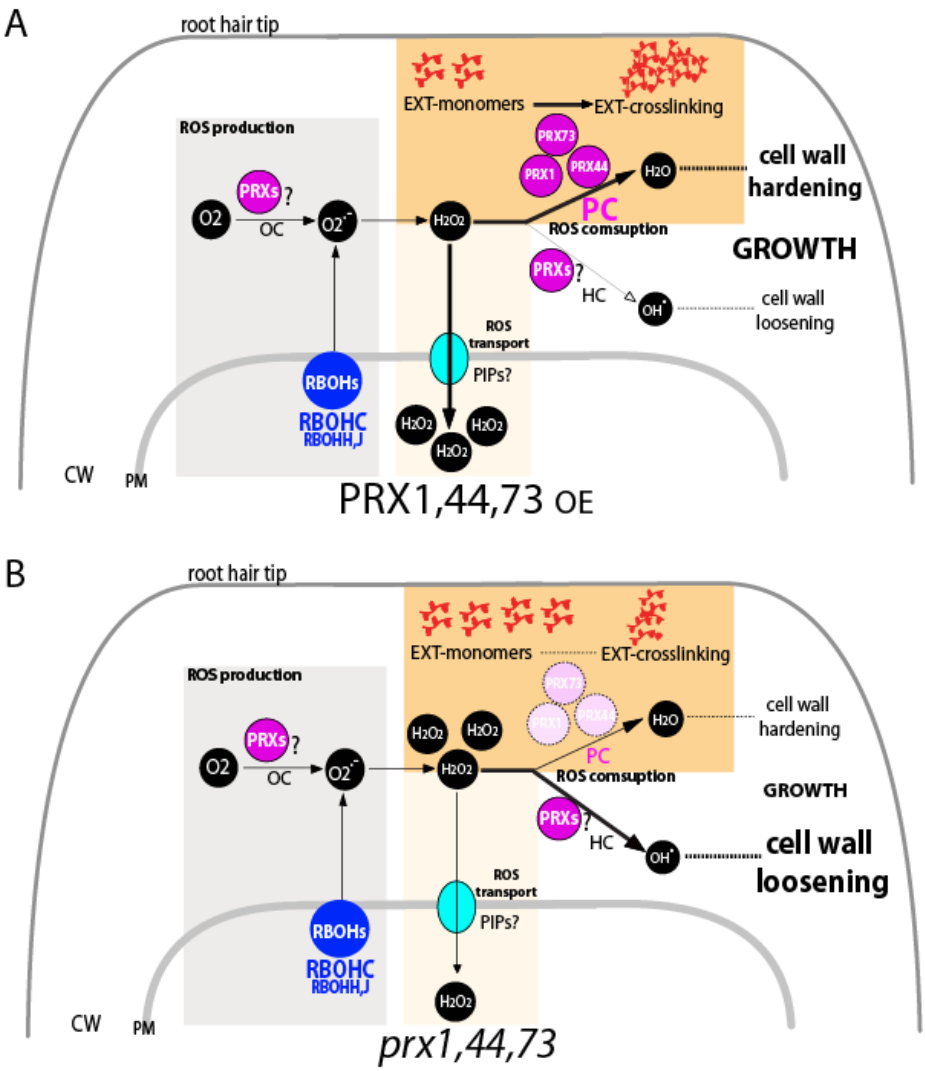

Figure S8. Current model of PRX01, PRX44, and PRX73 function on the ROS homeostasis linked to EXT-crosslinking in the root hair cell walls. ROS homeostasis in the apoplast includes ROS production, ROS consumption, and ROS transport to the cytoplasm. ROS as superoxide ion ($O2^-$) is primarily produced by RBOHC and by RBOHH,J (based on Mangano et al. (2017) and, possibly, by unknown PRXs in the root hair tip, and then dismutated to hydrogen peroxide (H_2O_2). (**A**) It is proposed that under high levels of PRX01,44,73 (in OE lines), this might trigger during the peroxidative cycle (PC) a high consumption of apoplastic H_2O_2 and the crosslinking of EXT-monomers at Tyr-units to allow the formation of the EXT-network and a concomitant cell wall hardening. A portion of the apoplastic H_2O_2 might be transported into the cytoplasm by aquaporins (PIPs). (**B**) In the triple mutant *prx01,44,73*, most of the H_2O_2 produced is accumulated in the apoplast-cell walls and most of the EXT monomers are not cross-linked. The balance between cell wall hardening and cell wall loosening processes might be compromised impacting on polar root hair growth. CW= cell wall, PM= plasma membrane; HC= Hydroxylic Cycle; OC= Oxidative Cycle.